Journal of Industrial and Mechanical Engineering

Volume No. 9

Issue No. 2

May - August 2025

ENRICHED PUBLICATIONS

ENRICHED PUBLICATIONS PVT. LTD

S-9, IInd FLOOR, MLU POCKET,
MANISH ABHINAV PLAZA-II, ABOVE FEDERAL BANK,
PLOT NO-5, SECTOR-5, DWARKA, NEW DELHI, INDIA-110075,
PHONE: - + (91)-(11)-47026006

Journal of Industrial and Mechanical Egineering

Aims and Scope

Journal of Industrial and Mechanical Engineering is a peer-reviewed journal for the presentation of original contributions and the exchange of knowledge and experience on mechanical and industrial engineering topics like Acoustics and Noise Control, Aerodynamics, Agricultural machinery, Applied Mechanics, Automation, Mechatronics and Robotics, Automobiles, Automotive Engineering, Ballistics, Biomechanics, Biomedical Engineering, Composite and Smart Materials, Composite Materials, Compressible Flows, Computational Mechanics, Computational Techniques, Dynamical Analyses, Dynamics and Vibration, Energy Engineering and Management, Engineering Materials, Fatigue and Fracture, Fluid Dynamics, Fluid Mechanics and Machinery etc.

Journal of Industrial and Mechanical Engineering

Journal of Industrial and Mechanical Engineering

(Volume No. 9, Issue No. 2, May - August 2025)

Contents

Hydraulic Behaviour of Auxiliary Devices For Rapid Mixing

Suresh Kumar, N[1], Pani, B.S.[2], Joshi, S.G.[3]

[1] Prof., Department of Civil Engg., College of Engg., Osmania University, Hyderabad-500 007, Telangana, India. Phone: 040-27097125; Fax: 040-27090317; e-mail: nskdr@yahoo.co.in

[2]Prof(Retd), Department of Civil Engg., IIT., Bombay-400 076, e-mail: bspani@iitb.ac.in

[3]Prof(Retd), Department of Civil Engg., IIT., Bombay-400 076, e-mail: bspani@iitb.ac.in

A B S T R A C T

Rapid mixing is an operation by which the coagulant is rapidly and uniformly dispersed throughout the volume of water and creates a more or less homogeneous system. Hence, attempts were made to improve the mixing process. Two kinds of devices viz., a circular disc and cross vanes were used as aids to free jets, to inject coagulants into the mixing chamber. The study had indicated that there is no significant improvement in the mixing process.

Keywords: *Rapid mixing, hydraulic behaviour, detention time, mixed flow, and dead space*

1. Introduction

In many water and wastewater treatment processes, mixing is required to blend one substance uniformly with another. Depending on the objective of the unit process and physical set-up mixing of liquids can be accomplished by a number of methods. In rapid mixing, chemical additives must be blended with receiving stream to form a homogenized mixture. This process differs significantly in purpose and criteria from the subsequent stirring process or flocculation, which is accomplished over a longer period. A combination of mixing and agitation that produces aggregation is called 'flocculation', even though more specific terms such as coagulation and flocculation are commonly used.

The primary function of rapid mixing is to instantly and uniformly disperse chemicals in the total volume of water. A rapid mixing device should be simple, practical, and relatively inexpensive and should not create appreciable head losses.

Designers traditionally select residence times for characterization of rapid mixing, flocculation, and the settling basins. They reflect the provision of appropriate volumes for achieving the related functions. The selections of residence time may be based on experience gained from jar tests conducted at the plant site. The important factors influencing the residence time are the dead space, plug flow, and the mixed flow.

2. Objectives of the study

In a rapid mixing chamber one would wish to get as high a value as possible for the mixed flow. Therefore, it was felt that this could perhaps be improved by suitably changing the inlet conditions into the chamber. Hence, it was decided to study the hydraulic behaviour of the tanks to assess the increase in the percentage of mixed flow with the two simple devices shown in Fig.1 and Fig.2. The description of these devices is given below:

i) cross vanes of 75 mm x 25 mm long with nominal thickness : these vanes were installed in the influent pipe leading to the rapid mixing chamber. This was to generate more shear in the jet for ensuring better entrainment and mixing. The vanes were kept 50 mm (twice the nozzle diameter) ahead of the jet inlet into the rapid mixing chamber.

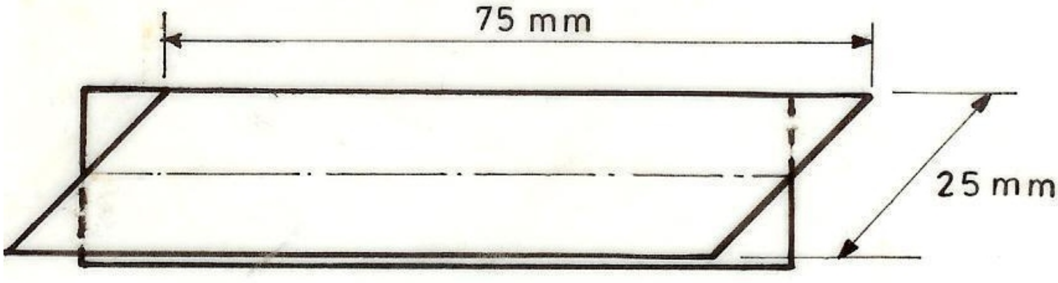

FIG.1 DETAILS OF CROSS VANES

ii) a circular disc of 75 mm diameter : this was kept to act as a jet deflector at a distance of about half of the nozzle diameter (12.5 mm) from the jet outlet. The diameter of the disc was three times the nozzle diamter. On conducting some initial runs it was observed that the zone just behind the circular disc was not taking part in the mixing process. Hence, to overcome this problem a concentric opening having a diameter slightly less than the jet diameter (keeping in view of the practical limitations) was made in the circular disc.

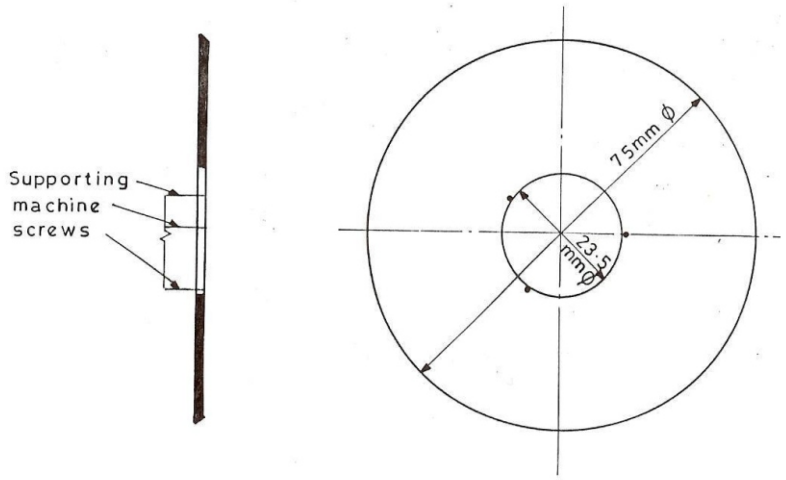

FIG.2 DETAILS OF A JET DEFLECTOR

The aim of the present investigation was to examine the hydraulic behaviour of proposed devices to aid the rapid mixing. Therefore, it is essential to see that there is least physical restriction to the flow stream. Moreover, it should be convenient to handle for operation and maintenance purposes.

A free jet for mixing purposes plays a dual role. It inserts a relatively small quantity of the fluid to be mixed, and also acts as a mixer. This stirring action by jet results in an increase in the homogeneity of the fluid. Rapid mixing through free jets does not involve any kind of mechanical components. Hence, the system is free from all the troubles associated with mechanical equipments. Therefore, the maintenance cost of these systems could be negligible.

In rapid mixing, the intensity of mixing is dependent upon the mean velocity gradient G. This is defined as the rate of change of velocity per unit distance normal to a section (Camp and Stein, 1943). Mathematically it is expressed as,

$$G = \left(\frac{P}{\mu V} \right)^{1/2} \tag{1}$$

G = mean velocity gradient, P = total input power, μ = absolute viscosity of water
V = volume of water to which power is applied

3. Description of experimental set-up

Complete details of the experimental set-up are shown in Fig.3 and Fig.4. The mixing chamber was fabricated out of acrylic sheets for viewing purposes. Raw water stored in a tank was pumped to the mixing chamber with the help of a pump. The required flow rate was obtained by adjusting the valve 1, while the surplus water was diverted back to the raw water tank through valve 2. The inlet to the mixing chamber was a submerged jet emanating from the influent pipe. The outlet was a suppressed sharp crested weir whose crest level could be adjusted. The rate of flow entering the mixing chamber was measured volumetrically in a collecting tank.

To obtain the total energy on the up-stream side of the mixing chamber, pressure tappings were provided on the pipe leading to the chamber. To know the head over the outflow weir a pressure tapping was provided in one of the adjoining sidewalls of the chamber. All pressure head measurements were made with reference to the centre line of the influent pipe to the mixing chamber.

The jet size selected was 25 mm in diameter and velocity of the efflux section varied from 3 to 4.5 m/s. The flow rates corresponding to the detention times of 40, 50, 60, and 90 seconds were 2.21, 1.767, 1.473, and 0.9817 lps respectively. The plan shapes of the mixing chamber chosen for the present investigation were square, circular, triangular (equilateral), and pentagon for the same plan area of 1963.5 sq. cm., and a liquid depth of 450 mm.

It has been recommended that in case of tanks provided for the sole purpose of mixing the liquid level in the tank should be less than 1.25 times the diameter of the tank. Otherwise it may require either multiple impellers or excessive power for proper mixing (Holland and Chapman, 1966). According to Maruyama (1986), for mixing by a horizontal jet the optimum depth of submergence of the nozzle is three quarters of liquid depth, when the depth is equal to the tank diameter. When liquid depth is smaller than the tank diameter, the nozzle should be located at mid depth. For horizontal position of the nozzle the mixing time was less than that obtained by tilting the nozzle at different angles of inclinations.

In the present study the liquid level in the tank was kept less than the diameter (or the length of the sidewall as the case may be) of the tank. Hence, the jet was injected at 50% of liquid depth.

4. Tracer studies

Tracer studies are conducted to mixing, flocculation, sedimentation or other processes in which residence time needs to be evaluated or controlled. There are two ways of applying tracer substances to obtain residence times in treatment plants. They are pulse / slug dosage and step dosage.

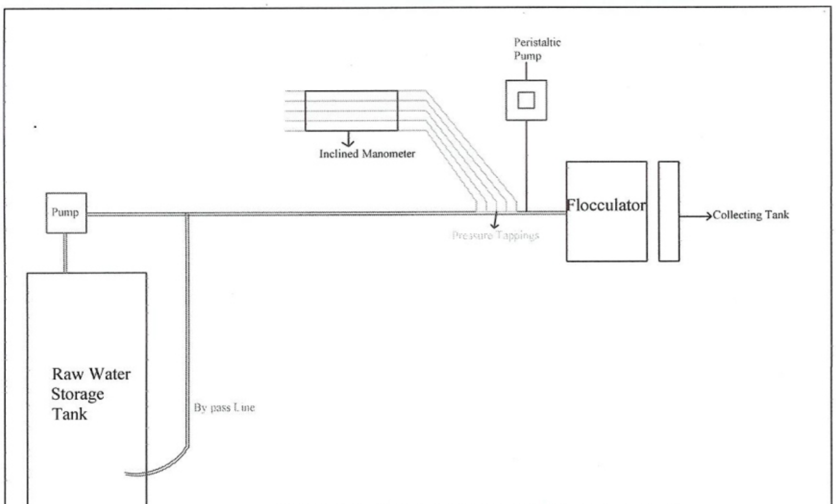

FIG 3 - LAYOUT OF THE EXPERIMENTAL SET-UP

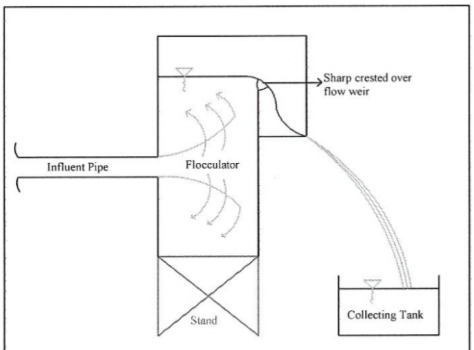

FIG 4 - DETAILS OF A JET FLOCCULATOR

In the present investigation, sodium chloride was used as a tracer to know the residence time distribution. Tracer solution was injected into the chamber through a vertical seamless stainless steel tube of 3 mm diameter just after the jet exit from the nozzle. In another arrangement, the tracer solution was injected into the influent pipe line as a co-current axial jet just before the main jet enters the rapid mixing chamber. The degree of mixing was observed to be the same in both these cases. The former arrangement is superior to the latter one from the maintenance point of view. However, in the present study the latter arrangement was used for the convenience of experimentation. Tracer studies were conducted in the selected plan shapes to examine the efficacy of proposed devices for rapid mixing.

After the injection of salt solution, its concentration near the outlet of the chamber was determined initially for every 10 seconds and subsequently at every 15 seconds intervals after the injection of tracer solution. The sampling was continued till the tracer disappeared from the collected samples. The sodium concentration in the samples was measured with the help of a digital conductivity meter. Experiments were repeated three times to examine the repeatability of the tank behaviour.

Tracer studies were conducted to observe the hydraulic behaviour of the above two devices in different plan geometries. A typical flow-through curve is shown in Fig.5. The dimensionless exit age distribution function (E) is plotted against the reduced time (). From Fig.5 it is clear that, both the devices have showed almost the same kind of hydraulic behaviour. A material balance check was carried out to verify the recovery of the tracer material added. In the present investigation this error ranged between +1.5% and +4.5%. This error could be because of experimentation.

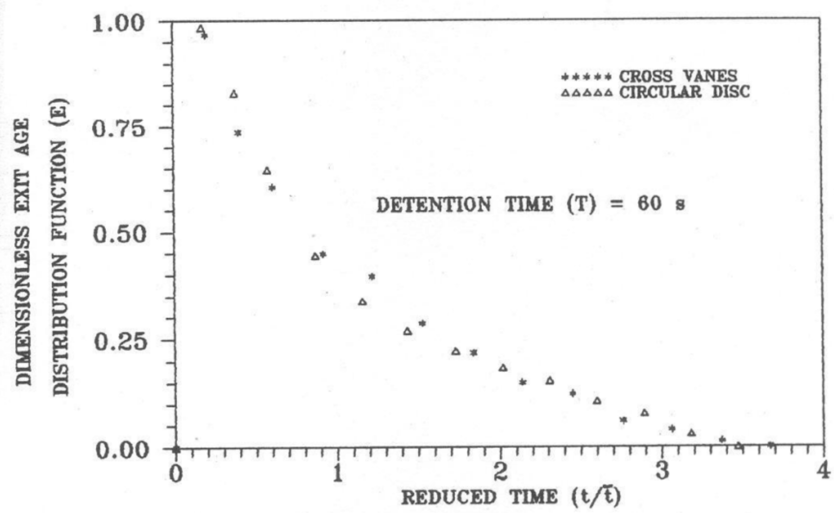

FIG.5 TRACER TEST RESULTS IN A SQUARE TANK

The important residence time characteristics viz., plug flow, mixed flow, and dead space were determined making use of the procedure given below (Rebhun and Argaman, 1965):

$$1 - F(t) = \exp - \left(\frac{1}{(1-p)(1-m)} \right) \left(\frac{t}{T} - p(1-m) \right) \quad (2)$$

F(t) = fraction of the applied dosage measured in samples at basin outlet, for each value of time t

T = detention time = V/Q

Q = rate of flow

p = fraction of active flow volume acting as plug flow

1-p = fraction of active flow volume acting as mixed flow

m = fraction of total basin volume that is dead space

1-m = fraction of total basin volume that is effective

Correspondingly, 1- F(t) represents the fractional part remaining longer than t. The degree of mixing was evaluated from the percentage of mixed flow. Residence time distribution of the tracer material with the proposed devices in a square tank is shown in Fig.6. The results of present study could not be compared with any other data because no information is available on the hydraulic behaviour of tanks for rapid mixing. The important residence time characteristics and other flow parameters are given in Table1. It is seen that the degree of mixing is almost the same regardless of the plan shape of the reactor for both the devices.

5. Results and Discussion

A higher value of mixed flow indicates that there is more uniform mixing of fluid, which is required in rapid mixing. In a chamber containing dead pockets the tracer may diffuse into these regions during the early stages of the run and might ooze out slowly in the latter stages. Hence, the time-concentration curve recession limb may become unduly elongated in the form of the long tail. This might also result in the shift of mean residence time about the centroid of the flow-through curve.

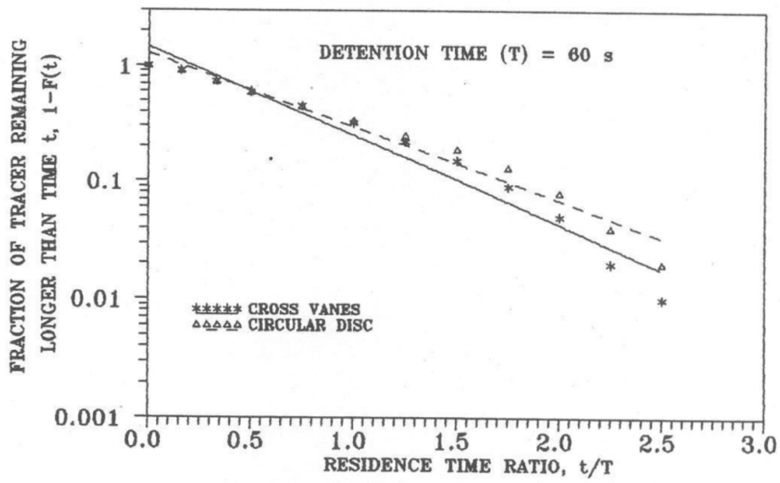

FIG.6 RESIDENCE TIME DISTRIBUTION IN A SQUARE TANK

Table 1. Results of tracer studies

		Cross vanes			Circular disc		
Description	Detention time (s)	Plug flow (%)	Mixed flow (%)	Dead space (%)	Plug flow (%)	Mixed flow (%)	Dead space (%)
Square		31.96	68.04	23.42	29.00	71.00	26.62
Circular		27.80	72.20	18.21	31.35	68.65	26.00
Triangular (e)	40	31.06	68.94	25.05	29.33	70.67	26.28
Pentagon		30.87	69.13	26.52	30.71	69.29	25.43
Square		25.75	74.25	15.79	22.04	77.96	18.12
Circular		29.00	71.00	18.66	26.48	73.52	17.31
Triangular (e)	50	29.38	70.62	21.91	28.09	71.91	15.46
Pentagon		24.56	75.44	17.69	23.48	76.52	19.42
Square		27.61	72.39	22.02	20.00	80.00	15.88
Circular		20.08	79.92	20.13	28.52	71.48	14.95
Triangular (e)	60	26.38	73.62	17.43	26.23	73.77	19.36
Pentagon		23.14	76.86	26.56	22.91	77.09	29.59
Square		26.6	73.4	34.33	26.80	73.20	32.38
Circular		29.87	70.13	28.80	22.19	77.81	27.45
Triangular (e)	90	29.64	70.36	29.04	29.64	70.36	29.04
Pentagon		25.69	74.31	36.89	24.76	75.24	37.68

From the Fig.6 it is evident that, the data can be best fitted in the range of t/T = 0 and 2. After t/T = 2 the best fit becomes curvilinear. This shift in the slope of the line could be because of the above mentioned phenomenon i.e., the slow release of the tracer material from the dead zones present in the chamber resulting in the longer recession limb of the flow-through curve. Almost the same trend was observed in all the experiments of the present investigation.

The percentage of mixed flow values lied in the range of 72 to 82 for various plan shapes in the selected detention times (Suresh Kumar, 1997). From the results of Table 1 it is evident that, for both the cross vanes and a circular disc the percentages of mixed flow ranged between 68 and 80. Further, they have increased the dead space fraction considerably (10 to 20%). In a rapid mixer a high percentage of dead space would lead to less effective utilization of coagulant and this will be reflected in the flocculator with a poor efficiency in the removal of suspended solids. Hence, a nozzle without any contraction is more effective from both hydraulic and maintenance point of view.

6. Conclusions

From the results of tracer studies it was observed that, the cross vanes and the circular disc have indicated almost same kind of hydraulic behaviour for the selected plan geometries. Further, these devices have increased the dead zones significantly (10 to 20%) in different plan geometries. Therefore, a jet without any contraction is simpler in arrangement and superior in performance over the proposed devices.

References

- *Camp, T. R., and Stein, P. C. (1943), Velocity gradients and internal work in fluid motion, J. Boston Soc. Civil Eng. 30 : 219-237*
- *Holland, F. A., and Chapman, F. S. (1966), Liquid mixing and processing in stirred tanks, Reinhold Publishing Corporation, Chapman and Hall Ltd., London : 1-65*
- *Maruyama Toshiro (1986), Jet mixing of fluids in vessels, Encyclopedia of Fluid Mechanics vol. 2 edited by Cheremisinoff, N.P., Gulf Publishing Company book division, Houston, Texas : 544-556*
- *Rebhun, M. and Argaman, Y.(1965), Evaluation of hydraulic efficiency of sedimentation basins, J. San. Engg., ASCE, 91(5) : 37-45*
- *Suresh Kumar, N (1997). Jet Mixing in Flocculators, Ph. D. thesis, Dept. of Civil Engg., IIT., Bombay*

Impact of Water Conservation Strucrures on Hydrology of A Watershed

Arpit Chouksey[1], Vinit Lambey[2], Shiv Prasad Aggarwal[3]

[1,3] Scientist/Engineer, Water Resources Department, IIRS, 4 Kalidas Road, Dehradun, 248001, India

[2]M.Tech. Student, Water Resources Department, IIRS, 4 Kalidas Road, Dehradun, 248001, India

Email: arpit@iirs.gov.in; Telephone No.: 0135-2524155

A B S T R A C T

A few areas of watershed are responsible for the high amount of water discharge and sediment flow. Providing the water conservation structures in these areas will be helpful in maintaining the desired flow requirement by reducing the total water and sediment yield. In this study, Jonk River, a tributary of Mahanadi basin has been selected to assess the impact of conservation structures. The outlet of Jonk River is located near Rampur in Chhattisgarh. Total area of the watershed is computed as 3424 km^2. Soil And Water Assessment Tool (SWAT) has been used to calculate the discharge and sediment flow on daily and monthly basis for the year of 2001 considering two case scenarios i.e. with and without ponds as conservation structure. For both the cases, the SWAT model has been setup with the observed precipitation and other global weather database available at SWAT website.

The simulated discharge and sediment flow data (Case-I) has been compared with the observed data and the correlation coefficient is found to be 0.84 & 0.77 respectively. The annual discharge and sediment flow value in "with pond scenario" has been detected to be reduced by 69.27 % and 64.10 % respectively when compared to "without pond scenario". The results observed in the present work can be used for site suitability analysis of soil and water conservation structures in the areas those are prone to soil erosion and floods. The study also reveals that the SWAT model can be use efficiently for the selection and application of best management practices (BMP).

Keywords: *Watershed, SWAT, sediment flow, Discharge*

Introduction

Water is an essential element for survival of living things. It is vital factor for economic development and increasing growth of agriculture and industry. To deal with water management issues, one must analyze and quantify the different elements of hydrologic processes taking place within the area of interests. A watershed is comprised of land areas and channels and may have lakes, ponds or other water flow of water on land areas occurs not only over the surface but also below it in the unsaturated zone and further below in the saturated zone[1]. The development over remote sensing (RS) techniques and Geographic Information System (GIS) capabilities has improved the expanded use of watershed models worldwide. GIS is a suitable tool for the efficient management of large and complex database and to provide a digital representation of watershed characteristics used in hydrological modeling. It has improved the efficiency of modelling process and ultimately increased the estimation capabilities of hydrological modeling [2]. Hydrological models such as MIKE-SHE, TOPMODEL, HEC-HMS, VIC, IHDM, WATFLOOD and SWAT, are capable of simulating spatio-temporal variations in hydrological processes. Many previous studies have demonstrated the ability of SWAT in detecting the impacts of landuse and climate change on hydrological components in different areas [3], [4], [5], [6], [7]. SWAT model is physically based, efficient and capable of continuous simulation for a long period. Therefore, SWAT model has been chosen to simulate or estimate the changes in runoff and sediment yield overdaily, monthlyand annual time scales.

In the present study SWAT Model is used to assess the impact of small water conservation structures over discharge and sediment yield. Jonk watershed, which is a part of Mahanadi basin has been selected as study area. The model has been run for two case scenarios i.e. watershed with pond as conservation structures and watershed without ponds or any conervation structure. The study has been carried out for the year 2001. However more emphasis was given to the monsoon season.

Study Area

The Jonk watershed is selected as study area which lies between geographic latitude 20^0 28' to $21^0$44' N and longitudes 82^0 20' to 83^0 00' E. The river Jonk originates from Nuapada district of Orissa at an elevation of 700 m from MSL (Fig. 1). It merges with Seorinarayan, upstream of Hirakud Dam after travelling the distance of 182 km having a drainage area of 3424 km^2.

The climate of the area is characterized by hot summer except during southwestern monsoon. The watershed receives about 90% of the rainfall during monsoon which is active from middle of June to the end of the September. Normal maximum temperature is 43^0 C and minimum temperature is 10^0 C (CWC). Geologically, the watershed consists of gneiss rock formation. The sub-basin comprises of alluvial formation of various thickness.

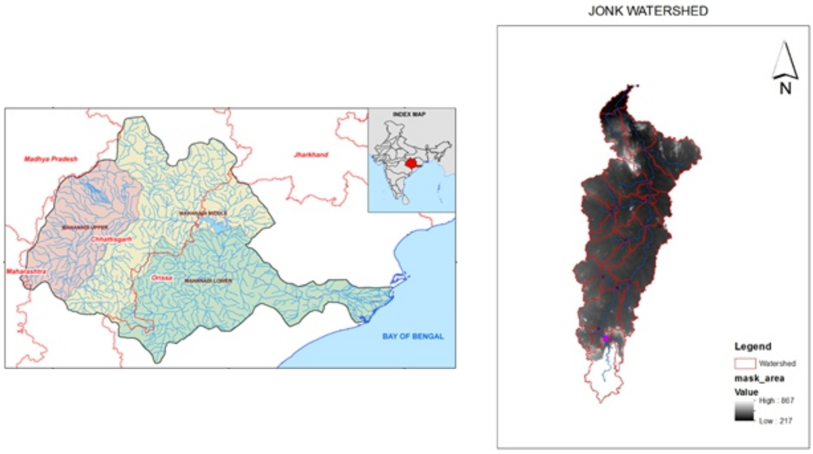

Fig 1. Jonk Watershed

Material & Methods

SWAT is semi-distributed, partially physically based, data driven model and requires several types of data such as rainfall, temperature, land use, soil, wind velocity, etc. [9]. Data has been collected from various sources and the post-processing have been carried out on the datasets as mentioned below.

(i) Land use database:

The land use map has been derived from the FCC image of Landsat 8 using maximum likelihood method under supervised classification. The image was re-projected using ArcGIS software.

(ii) Soil database:

Soil dataset has been downloaded from FAO (1981) website [8]. The necessary input information required by the SWAT model was extracted from the same database for each soil type, namely soil texture, Hydrological Soil Group (HSG).

(iii) Weather database:

SWAT requires daily values for precipitation, maximum and minimum temperature, solar radiation, relative humidity and wind speed for modeling of various physical processes, soil and rainfall being the most important. Daily meteorological data was collected from Indian Meteorological Department.

(iv) SWAT project:

Firstly, ASTER dem (resolution: 30m) was converted from geographic coordinate system to projected coordinate system (UTM, datum: WGS84). After this, it has been imported to SWAT project to start watershed delineation. After importing to SWAT project, stream are defined based on the drainage area threshold. The outlet for the whole watershed has been defined near Rampur and watershed delineation has been done. After delineation, sub basin parameters are calculated with locating the positions of the reservoirs. For each sub basin land use data and soil data are defined. As the runoff depends on the actual hydrologic conditions of each land cover and soil present in the watershed, therefore impact of each landuse is considered. HRU is defined as 20% for landuse, slope and soil class for each sub basin. One of the main sets of input for simulating the watershed in SWAT is climate data. Climate inputs consist of precipitation, maximum and minimum temperature, solar radiation, wind speed and relative humidity. The daily precipitation records of 2001 were used which were analyzed to develop the climate-input files required for the model.

After addition of all the above data, the SWAT model is set up and run on the basis of daily and monthly simulation. Whole process of the above method is explained in the flow chart below.

In this case study, the main emphasis is to detect the reduction of discharge and sediment flow in the Jonk watershed by addition of ponds as water conservation structures. In SWAT, runoff volume is estimated from daily rainfall using the modified SCS-CN (Curve Number Method, Eq. 1) and Green-Ampt methods. The SCS-CN equation is:

$$Q_{surf} = \frac{(R_{day}-I_a)^2}{(R_{day}-I_a+S)} \qquad (1)$$

Where, Q_{surf} is accumulated runoff, R_{day} is rainfall depth for the day, I_a ia the initial abstractions commonly taken as (0.2*S), S is the retention parameter which is given as S = (25400/CN) - 254

The discharge is calculated with the help of rational formula which is written as:

$$Q_{peak} = \frac{C*i*A}{3.6} \qquad (2)$$

Where, Q_{peak} is the peak runoff rate (m^3/s), *i* is the rainfall intensity (mm/hr.), C is the runoff coefficient, A is area of the subbasin area (km^2) and 3.6 is the unit conversion factor.

Similarly, the sediment flow is obtained from the modified universal soil loss equation (MUSLE) which is given as:

$$Sed = 11.8 * (Q_{surf} * Q_{peak} * Area_{hru})^{0.56} * K_{USLE} * LS_{USLE} * C_{USLE} * P_{USLE} * CFRG \quad (3)$$

Where, Sed is the sediment yield on given day (metric tons), Q_{surf} is the surface runoff volume (mm/ha), Q_{peak} is the peak runoff rate (m^3/s), $Area_{hru}$ is area of HRU (ha), K_{USLE} is the USLE soil erodibility factor, LS_{USLE} is the USLE topographic factor, C_{USLE} is USLE cover and management factor, P_{USLE} is USLE land practice factor, CFRG is coarse fragmentation factor.

The methodology followed for the study is given is Fig. 2.

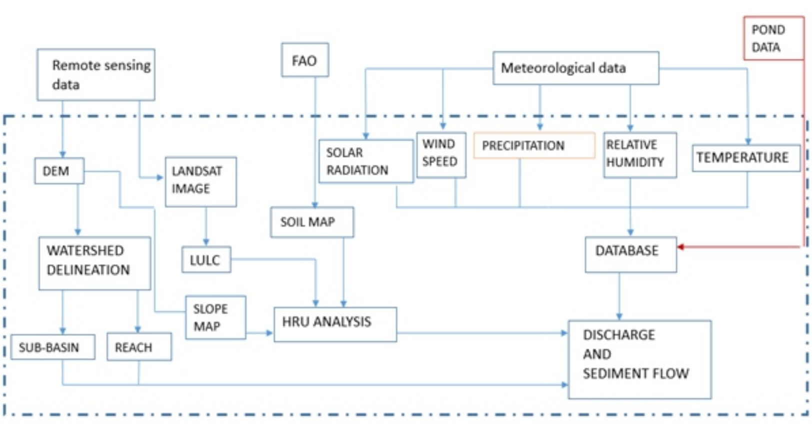

Figure 2. Methology Flow Chart

Figure 3, 4, 5 & 6 shows the drainage network map, landuse/landcover, HRU and slope map of the watershed.

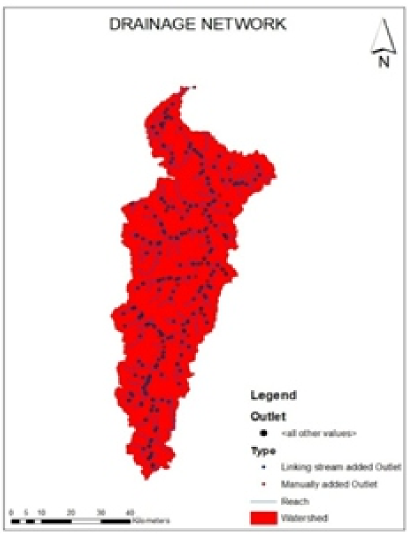

Figure 3. Drainage Map

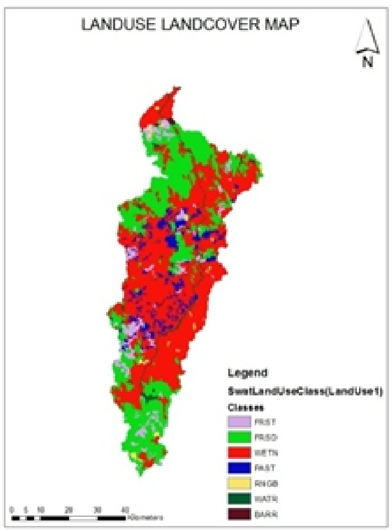

Figure 4. Landuse/Landcover Map

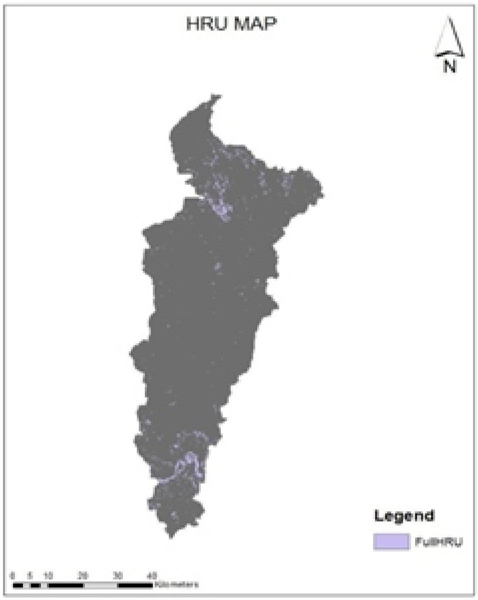

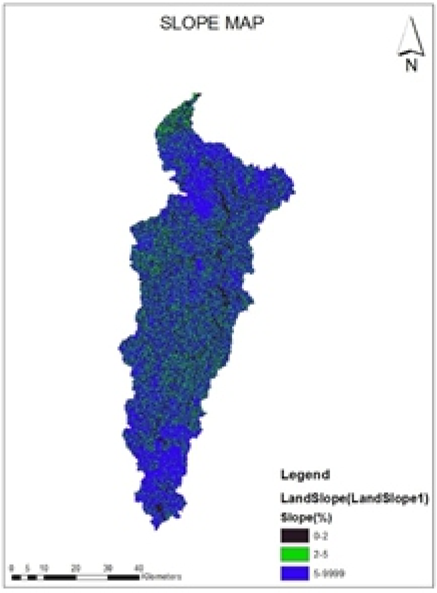

Figure 5. HRU Map

Figure 6. Slope Map

Results

A physically based SWAT model has been used for assessment of the impact of small water conservation structures on hydrology of a watershed and the results obtained are quite satisfactory. Here, the results are shown for the period of July to October i.e. only for monsoon season.

Fig. 7 and Fig. 8 shows the maximum daily discharge and sediment flow in jonk watershed is found to be 2.97 cumecs and $1.937 x 10^5$ t/ha/yr respectively for the year 2001 when there was no pond as water conservation structures and the same is reduced to 1.984 cumecs and $0.29 x 10^5$ t/ha/yr. due to presence of pond . The maximum monthly discharge and sediment flow is also observed to be decreased from 2.13 cumecs to 1.25 cumecs and $5.05 x 10^5$ to $1.22 x 10^5$ t/ha/yr respectively, due to addition of pond as water conservation structures as shown in fig. 5. The comparison of different parameters with the both case scenarios is shown as the table below

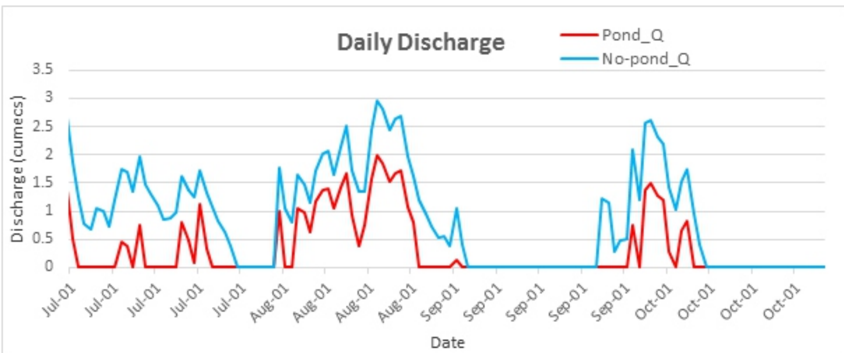

Figure 7. Simulated Discharge for Case-I and Case-II

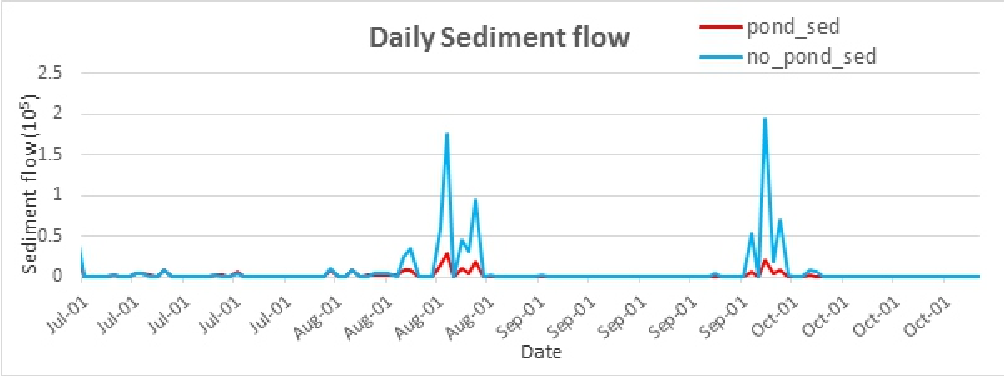

Fig. 8. Simulated Sediment Flow (t/ha/yr) in both scenarios

Annual water balance components are shown in Table 1. In the table, it is clear that seepage increases with the effect of ponds or small water conservation structures, hence deep aquifer recharge is increased.

Table 1. SWAT model Standard Output Parameters

Without pond	With pond
PRECIP = 768.7 MM	PRECIP = 768.7 MM
LATERAL SOIL Q = 29.31 MM	LATERAL SOIL Q = 30.84 MM
GROUNDWATER (SHAL AQ) Q = 0.00 MM	GROUNDWATER (SHAL AQ) Q = 0.18 MM
GROUNDWATER (DEEP AQ) Q = 0.22 MM	GROUNDWATER (DEEP AQ) Q = 0.88 MM
DEEP AQ RECHARGE = 0.38 MM	DEEP AQ RECHARGE = 1.56 MM
TOTAL AQ RECHARGE = 7.58 MM	TOTAL AQ RECHARGE = 31.25 MM
TOTAL WATER YLD = 106.72 MM	TOTAL WATER YLD = 130.25 MM
PERCOLATION OUT OF SOIL = 7.85 MM	PERCOLATION OUT OF SOIL = 32.35 MM
TOTAL SEDIMENT LOADING = 1.499 T/HA	TOTAL SEDIMENT LOADING = 1.453 T/HA

Discussions

SWAT model was calibrated for the Jonk watershed, with reasonable accuracy for monthly and daily discharge processes for one year. The study shows that the SWAT model is reliable for estimation of discharge and sediment flow. SWAT tool is compatible for watershed analysis and water management practices. The reduction in monthly discharge due to addition of water pond as water conservation structure is found to be 41 - 89 %. The reduction in monthly sediment flow due to addition of water pond as water conservation structure is found to be 32 - 88 %. Due to addition of the water conservation structures, the flow of sediment is reduced which results in less soil erosion and also the capacity of reservoir will increase. Deposit of sediments will increase the percolation of the water in the ground results increase in ground water recharge. The reduction in discharge of water due to pond construction will be helpful during non-rainy days. The results observed in the present work can be used for site suitability analysis of soil and water conservation structures in the areas which are prone to soil erosion and floods.

Conclusion

The annual mean reduction of the discharge due to water conservation structures such as pond is found to be 69.27 % while mean reduction in sediment flow due to construction of pond is found to be 64.10 %. From the above study, it can be concluded that construction of small water conservation structures may be very helpful in controlling the discharge which can cause floods and controlling the sediment flow which causes the sedimentation of the reservoirs.

References

[1] V.P. Singh, D.K. Frevert, Mathematical Modeling of Watershed Hydrology. Chapter 1, in: Mathematical Models of Small Watershed Hydrology and Applications, Water Resources Publications, Littleton, Colorado, 2002, pp. 1–3.

[2] S.J. Bhuyan, J.K. Koelliker, L.J. Marzen, J.R. Harrington, An integrated approach for water quality assessment of Kansas watershed, Environ. Model. Softw. 18 (2003) 473–484.

[3] Fan, M., Shibata, H., 2015. Simulation of watershed hydrology and stream water quality under landuse and climate change scenarios in Teshio River watershed, northern Japan. Ecol. Indic. 50, 79–89

[4] Nie, W., Yuan, Y., Kepner, W., Nash, M.S., Jackson, M., Erickson, C., 2011. Assessing impacts of landuse and landcover changes on hydrology for the upper San Pedro watershed. J. Hydrol. 407 (1), 105–114.

[5] Gassman, P.W., Reyes, M.R., Green, C.H.,Arnold, J.G., 2007. The Soil andWaterAssessment Tool: historical development, applications, and future research directions. Trans. ASABE 50 (4), 1211–1250

[6] Guo, H., Hu, Q., Jiang, T., 2008. Annual and seasonal streamflow responses to climate and land-cover changes in the Poyang Lake basin, China. J. Hydrol. 355 (1), 106–122.

[7] Zhou, F., Xu, Y., Chen, Y., Xu, C.Y., Gao, Y., Du, J., 2013. Hydrological response to urbanization at different spatio-temporal scales simulated by coupling of CLUE-S and the SWAT model in the Yangtze River Delta region. J. Hydrol. 485, 113–125.

[8] FAO, 1981. United Nations Food and Agriculture Organization, Soil Map of the World, vols. 1–10 (1:5M scale maps). UNESCO, Paris.

[9] Z. Nasrin, G.A. Sayyad, S.E. Hosseini, Hydrological and sediment transport modeling in maroon dam catchment using soil and water assessment tool (SWAT), Int. J. Agron. Plant Prod. 4 (10) (2013) 2791–2795.

Creep Behavior and Creep Life Assessment of HP40NB Reformer Steel

***AmitavaGhatak, **P.S. Robi**
Department of Mechanical Engineering, Indian Institute of Technology Guwahati, Assam, India

A B S T R A C T

Centrifugally cast high Cr steels are widely used in petroleum and chemical industries as reformer tubes. In this paper, creep behavior of HP40Nb microalloyed tube steel has been examined at temperatures in the range of 1073 K – 1173 K at different stress levels. The creep deformation behavior follows the Dorn law equation. The constitutive creep equation was obtained using the data obtained from the accelerated creep tests. Following the Orr-Sherby-Dorn parametric technique, the creep life of the material at a service temperature of 1273 K was 10.7 years at a stress of 10 MPa.

Key Words: *HP40Nb steel, Creep, Activation energy, Orr-Sherby-Dorn parameter, Creep life.*

Introduction

HP40Nb microalloyed steel is used as reformer furnace tubes in chemical and petroleum industries for continuous production of hydrogen gas by catalytic reaction of hydrocarbons and steam [1-2]. The operating temperature of these tubes are generally in the range from 1073 K to 1273 K with an expected design life 10^5 h. Degradation of the microstructure resulting from the prolonged service exposure at high temperature and stress, many a times, results in premature failure of the tubes. This leads to forced shutdown of the plant and severe economic loss for the industry. A clear understanding of the creep behavior of the steel is required for a proper design of the components for the intended service life.

Material behavior during creep deformation is often complicated. Correlation between the applied stress(σ), test temperature (T) and minimum creep rate ε_m, are often expressed by constitutiveequations [3]. A number of different creep constitutive relationships have been proposed for modeling creep deformation behavior of metals and alloys [4]. Among the various constitutive equations, the widely accepted relationship is Dorn law [5] expressed as:

$$\varepsilon_m = A \exp \beta\sigma \quad \exp \ - \frac{Q}{RT} \qquad (1)$$

where A and β are constants, σ is applied stress in MPa, Q is the activation energy for creep in J/mol, R is gas constant (= 8.314J/ K- mol) and T is the absolute temperature in Kelvin. The constitutive parameters *i.e.* A, β and Q is determined from the creep test data.

Padilha et al. [6] studied the effect of precipitation behavior of 316L(N) stainless steel during creep test. Latha et al. [7] compared the creep properties of alloy D9 and 316 stainless steel in which alloy D9 exhibited higher creep rupture strength than 316L steel. The time independent plasticity and creep behavior of 316 stainless steel at 823 K was investigated by Hayhurst et al. [8] and the constitutive equation for creep deformation was obtained. Tahami et al. [9] compared creep behavior of cold drawn304L stainless steel using two different constitutive equations. Sawada et al. [10] predicted long term creep curve and proposed constitutive equations for various stainless steels. Damage characterization of HP40Nb steels after 10 years of service exposure at 1223 K was reported by Alvino et al. [11]. To the best of our knowledge, study related to creep behavior of the microalloyed HP40Nb reformer steel based on constitutive equation have not been reported.

Various creep rupture parametric techniques have been developed to predict the long-term creep life of high temperature components. These are mainly by Orr-Sherby-Dorn parameter [12], Larson-Miller parameter [13], Manson-Haferd parameter [14], Manson-Succop parameter [15] etc. Among these, Orr-Sherby-Dorn parametric ($P_{O\text{-}S\text{-}D}$) technique is an accepted model and is expressed as:

$$P_{O-S-D} = \log_{10} t_r - \frac{Q}{2.3RT} \qquad (2)$$

where t_r is the rupture time in hours.

The present work is aimed at investigating the creep behavior and predicting the creep life of HP40Nb microalloyed steel by $P_{O\text{-}S\text{-}D}$ technique. Accelerated creep tests were carried out for various combinations of temperature and stresses. The data obtained from these experiments was used to develop the constitutive equations for creep deformation behavior.

2. Material and methodology

Material and specimen preparation

Material used for investigation was centrifugally cast reformer tube. The inside diameter and thickness of the tube are 106 mm and 15.3 mm, respectively. The chemical composition of the steel analyzed by optical emission spectrometer is shown in Table 1. Flat tensile creep specimens of 25 mm gauge length, 6.5 mm width and 3 mm, were machined by wire-cut electric discharge machining. The axis of the specimen was kept parallel to the longitudinal axis of the reformer tube.

Table 1. Chemical composition of the steel in wt. %.

C	Si	Mo	Cr	Ni	Nb	Ti	Fe
0.4	1.3	0.037	23.6	34.9	0.8	0.037	Balance

2.2 Creep test

Nine tensile creep tests were carried out at various combinations of stresses (47 MPa, 68 MPa and 80 MPa) and temperatures (1073 K, 1123 K, and 1173 K). The specimen was heated to the test temperature by an impedance heater. The temperature of the specimen was measured by an Infrared pyrometer and controlled within an accuracy of ± 3 K till failure of the sample. A high definition video camera was used for on-line recording of the specimen gauge length extension during the creep test. The digital frames extracted from the video recording were used to determine the time dependent creep strain by imageanalysis technique. The minimum creep rate ε_r for various combinations of temperatures and stresses were determined from the creep curve.

3. Results and discussion

Minimum creep strain rate

Fig. 1(a) and (b) show the semi-logarithmic plots of ε_r vs. temperature and ε_m vs. stress, respectively. The figures show that the value of ε_n increases with the increase in temperature and/or stress. In both the figures (Fig. 1(a) and (b)), the lines are the best least squares fit to the data points. From the figures, it can be seen that a linear relationship exists between the logarithm of ε_n and temperature or applied stress. The maximum and minimum ε_n values are 5.05×10^{-4} s^{-1} and 6.25×10^{-8} s^{-1} at 80 MPa/1173 K and 47 MPa/1073 K, respectively.

Rupture time

Fig. 2(a) and (b) show semi-logarithmic plots of creep rupture time t_r vs. test temperature and applied stress, respectively. The figures reveal that the rupture time of the steel increase with decrease in temperature and/or stress. The lines in Fig. 2(a) and (b), represents the best least squares fit to the data points. The maximum and minimum rupture times are 441728 s and 197 s at 47 MPa/1073 K and 80 MPa/1173 K, respectively.

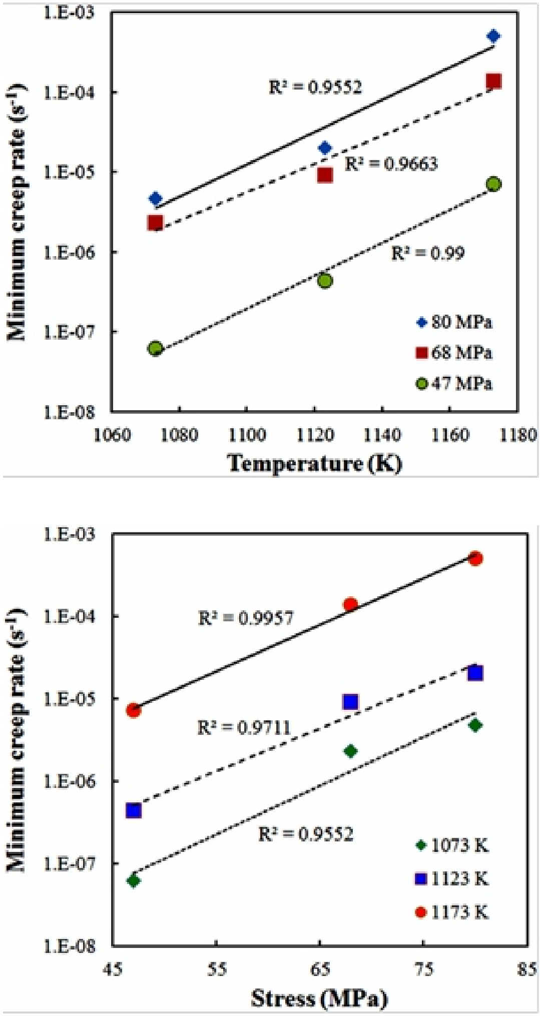

Fig 1. Plot of minimum creep ratevs. (a) temperature and (b) stress.

Constitutive equation

The values of ε_m obtained from creep curves were used to determine the constitutive parameters *viz.* constants A and β, and activation energy for creep Q, of Eq. 1. The constitutive parameters were determined by the least squares by minimizing the functional error e_i, between the experimental and predicted values of ε_m. The error e_i was defined by

$$e_i = \ln(\varepsilon_m \quad) - \ln A - \beta\sigma + \frac{Q}{RT} \tag{3}$$

where i is the number of observations. The three unknown parameters, A, B and Q of Eq. 1 was determined by minimizing the error. The values obtained for A, B and Q by the optimization technique is1.05×10^{13} s^{-1}, 0.52 and 468.5 kJ/mol, respectively.

(a)

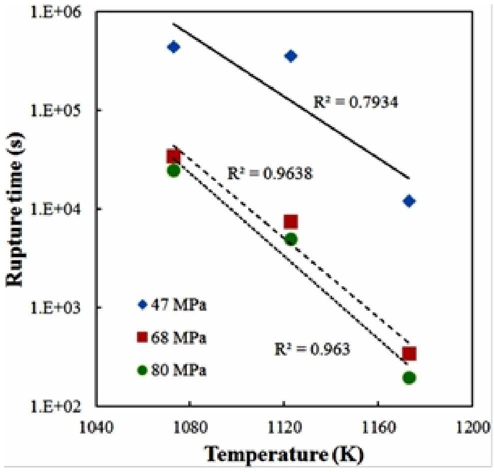

(b)

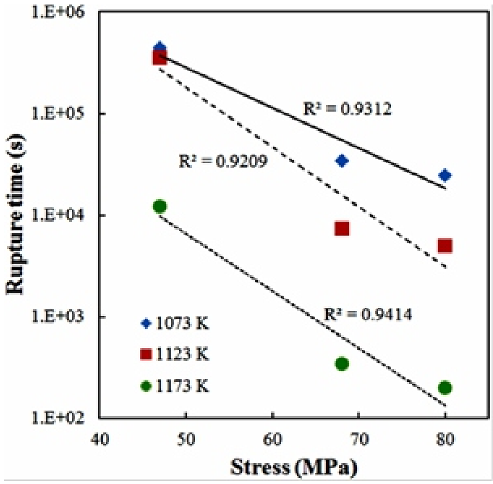

Fig 2. Variation of the rupture time with (a) temperature and (b) stress. Substituting these values in Eq.1, the constitutive equation for creep deformation within the domain of experimental conditions is expressed as:

$$\varepsilon_m = 1.05 \times 10^{13} \; exp \; 0.52\,\sigma \quad exp - \frac{468500}{RT} \tag{4}$$

The reported value of activation energy for lattice diffusion in austenitic steel is 270 kJ/mol [16]. In the present investigation, the activation energy for creep is found to be 468.5 kJ/mol. Higher activation energy obtained for the present material is due to the presence of carbides particles in the matrix which impedes the dislocation motion during the creep deformation.

The predicted minimum creep rate ε^{p}_{m} for combination of stresses and temperatures were determined using Eq. 4. Comparison of minimum creep rate obtained from the experiment ε^{e}_{m} and by Eq. 4 for 68 MPa and 80 MPa stresses are shown in Fig. 3. Experimental and predicted minimum creep rates at 68 MPa/1173 K are found to be 1.38×10^{-4} s^{-1} and 1.15×10^{-4} s^{-1}, respectively indicating a good agreement between experimental and the predicted values.

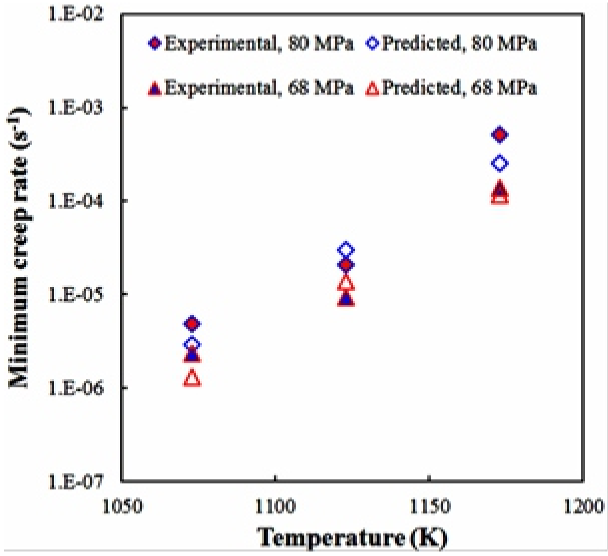

Fig. 3. Plot of minimum creep rate vs. temperature of experimental data and predicted data.

The semi-logarithmic plot of ε_{l} vs. σ for experimental data and calculated values for constant test temperatures are shown in Fig. 4. Predicted and experimental minimum creep rate values at 80 MPa/1073 K are 4.76×10^{-6} s^{-1} and 2.87×10^{-6} s^{-1}, respectively. Fig. 4 indicates good agreement between both experimental and calculated values of minimum creep rate.

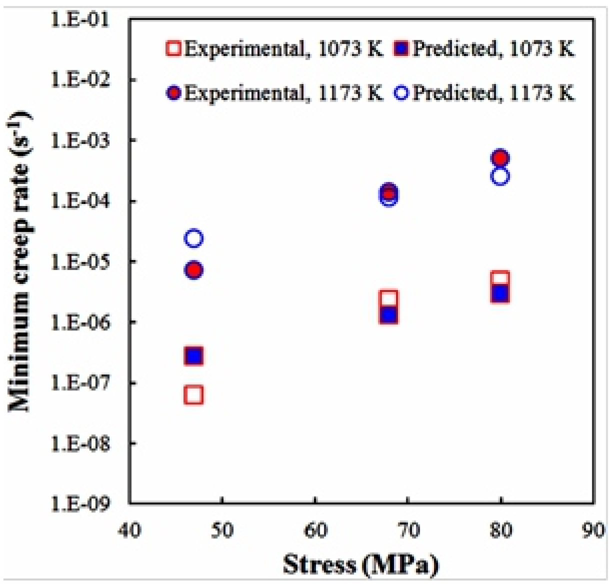

Fig. 4. Plot of minimum creep rate vs. stress of experimental data and predicted data.

The percentage error between $\ln(\varepsilon^{e}_{m})$ and $\ln(\varepsilon^{p}_{m})$was calculated. The maximum percentage error is found to be 14%, which is obtained for creep test at 47 MPa/ 1123 K. The result shows that Eq. 4 is indicative of the creep deformation behavior of the material within the domain of present experimental conditions.

Creep life prediction

Rupture time obtained from the accelerated creep test was used to calculate the Orr-Sherby-Dorn parameter $P_{O\text{-}S\text{-}D}$. In this technique, the activation energy for creep (Q = 468.5 kJ/mol) obtained from the constitutive model was used for the analysis. Fig. 5 shows the semi-logarithmic plot of $\sigma - P_{O\text{-}S\text{-}D}$, master curve for the investigated steel. The average value of $P_{O\text{-}S\text{-}D}$ for each stress levels was used to plot the master curve. In Fig. 5, the continuous line represents the trend line fitting the data points with a coefficient of determination $R^2 = 0.988$. The trend line was used for the extrapolation of $P_{O\text{-}S\text{-}D}$ values corresponding to a stress of 5 Mpa.

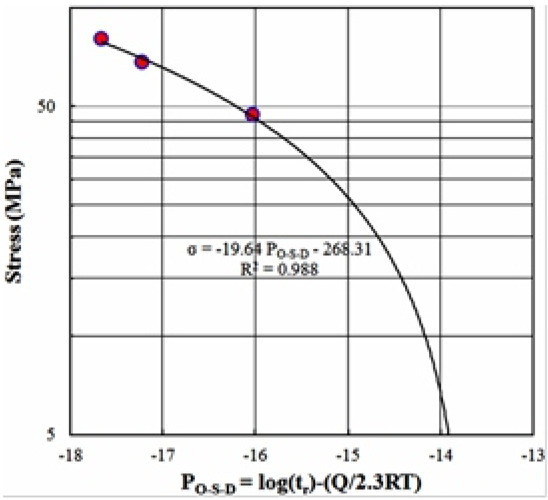

Fig. 5. Plot of stress vs. Orr-Sherby-Dorn parameter for the investigated steel.

The creep life of the steel was estimated from the master curve plot. $P_{O\text{-}S\text{-}D}$ values for the steel at stresses 5 MPa, 10 MPa, 15 MPa and 20 MPa were obtained by drawing horizontal lines corresponding to these stresses to meet the extrapolated curve and subsequently projecting to the $P_{O\text{-}S\text{-}D}$ axis. The respective values of $P_{O\text{-}S\text{-}D}$ for the above stresses obtained are -13.92, -14.17, -14.43 and -14.67. The creep life t_r of the steel for various temperatures were determined by substituting the $P_{O\text{-}S\text{-}D}$ values in the equation:

$$t_r = 10^{P_{O-S-D} + \frac{Q}{2.3RT}} \quad (5)$$

Fig. 6 shows the plots of creep life vs. temperature for the steel at different stresses. The plot indicates that the creep life of the steel increases with the decrease in temperature and /or decrease in stress. Life of the steel for a designed hoop stress of 10 MPa and at 1273 K is found to be 10.7 years.

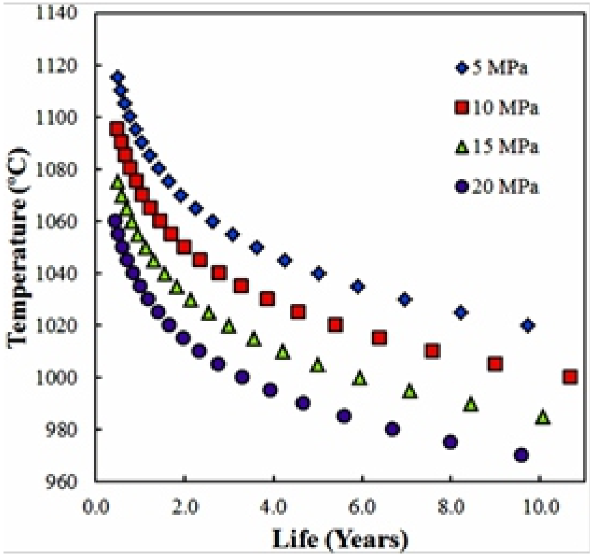

Fig. 6. Plot of temperature vs. life at different stresses of the steel.

The result of the study indicates that the material can be safely used at 1273 K/10 MPa for 11½ years. However, extreme caution should be taken so that the service conditions are not exceeded during the application.

4. Conclusion

Accelerated creep tests using constant stress creep setup have been carried out to analyze the creep behavior and to predict the creep life of the steel. Conclusions of the present investigation are summarized as follows:

- Minimum creep rate increases non-linearly with the increase in stress or temperature. Rupture time increases non-linearly with the decrease in stress or temperature.
- Dorn law equation provides an acceptable result to predict minimum creep rate. The value of A, β and Q are obtained as 1.05×10^{13} s^{-1}, 0.52 and 468.5 kJ/mol, respectively, for the investigated steel.
- Dislocation creep is the dominant deformation mechanism of the steel at higher temperature and stress.
- The creep rupture life of the steel has been evaluated by using the Orr-Sherby-Dorn parameter. A creep life of 10.7 years at 1273 K and 10 MPa was predicted by $P_{O\text{-}S\text{-}D}$ technique.

Acknowledgement

The authors wish to thank Numaligarh Refineries Limited, India for providing the reformer tube to carry out the study.

References

[1] GhatakA.and RobiP.S., "Effect of temperature on the tensile properties of HP40Nb microalloyed reformer steel", International Conference onProcessing and Fabrication of Advanced Materials XXII, Institution of Engineers Singapore (IES),Singapore, pp534-543

[2] WahabA.A. and KralM.V., 2005, 3D analysis of creep voids in hydrogen reformer tubes, Materials Science and Engineering A, 412(1-2),pp 222-229.

[3] SellarsC.M.and McTegartW.J., 1966, On the mechanism of hot deformation, Acta Metallurgica,14(9),pp1136-1138.

[4] HoldsworthS.R., AskinsM., BakerA., GariboldiE., HolmstromS., KlenkA., RingelM., Merckling G., SandstromR., SchwienheerM.and SpigarelliS., 2008, Factors influencing creep model equation selection, International Journal of Pressure Vessels and Piping, 85(1–2),pp 80-88.

[5] J. T. Boyle, and J. Spence, (1983) Stress Analysis for Creep, Butterworth & Company Ltd.

[6] PadilhaA.F., EscribaD.M., Materna-MorrisE., RiethM.and KlimenkovM., 2007, Precipitation in AISI 316L(N) during creep tests at 550 and 600 °C up to 10 years, Journal of Nuclear Materials, 362(1),pp 132-138.

[7] LathaS., MathewM.D., ParameswaranP., RaoK.B.S.and MannanS.L., 2008, Thermal creep properties of alloy D9 stainless steel and 316 stainless steel fuel clad tubes, International Journal of Pressure Vessels and Piping, 85(12), pp 866-870.

[8] HayhurstD.R., Vakili-TahamiF.and ZhouJ.Q., 2003, Constitutive equations for time independent plasticity and creep of 316 stainless steel at 550 °C, International Journal of Pressure Vessels and Piping, 80(2), pp 97-109.

[9] TahamiF.V., Daei-SorkhabiA.H.and BiglariF.R., 2010, Creep constitutive equations for cold-drawn 304L stainless steel, Materials Science and Engineering A, 527(18-19), pp 4993-4999.

[10] SawadaK., TabuchiM.and KimuraK., 2009, Analysis of long-term creep curves by constitutive equations, Materials Science and Engineering A, 510–511, pp 190-194.

[11] AlvinoA., LegaD., GiacobbeF., MazzocchiV. andRinaldiA., 2010, Damage characterization in two reformer heater tubes after nearly 10 years of service at different operative and maintenance conditions, Engineering Failure Analysis, 17(7-8), pp 1526-1541.

[12] OrrR.L., SherbyO.D.and DornJ.E., 1954, Correlations of rupture data for metals at elevated temperature, Transactions ASM, 46, pp 113-128.

[13] Larson F.R.and MillerJ., 1952, Time temperature relationship for rupture and creep stress, Transactions ASME, 74, pp 765-771.

[14] Manson S.S.and HaferdA.M., 1952,A linear time temperature relation for extrapolation of creep and stress rupture data, NASA TN2890.

[15] Manson,SSand Succop,G (1956). in: Stress-Rupture Properties of Inconel 700 and Correlation on the Basis of Several Time-Temperature Parameters, edited by ASTM, of Symposium on Metallic Materials for Service Temperatures Above 1600 F, ASTM-STP 174, ASTM,.

[16] ParkD.B., HongS.M., LeeK.H., HuhM.Y., SuhJ.Y., Lee S.C. and JungW.S., 2014, High-temperature creep behavior and microstructural evolution of an 18Cr9Ni3CuNbVN austenitic stainless steel, Materials Characterization, 93, pp 52-61.

Phonon-Phonon Interaction In Spectral Density Function of Semiconductor Crystals

S. C. Gairola

Department of Physics (School of Sciences), H. N. B. Garhwal University (A Central University) Pauri Campus, Pauri, Pincode-246001, Uttarakhand , India

A B S T R A C T

An electron Green`s function has been taken to develop the theory. Fourier transformed electron Green`s function has been evaluated with the help of equation of motion technique of quantum dynamics and Dyson equation approach.The response function has been provided the electron phonon linewidth and electron phonon shift from this technique. The perturbed mode energy has been dependent on electron band energy and electron phonon shift. The linewidth has been contributed by harmonic part, localized part, cubic, and quartic anharmonic parts. This study concludes that spectral density function has been contributed by harmonic part, electron part, defect part, cubic and quartic anharmonic parts. It has also been obtained that spectral density function shows a different delta function peaks which are affected by temperature and electron phonon coupling constant. It has been found that intensity of peaks have got sharper response when phonon frequency approaches to perturbed mode energy. The different excitations have been created in the form of exciton, polaron, combination, and difference bands. These have been responsible to broaden the delta function peaks. The different limiting cases of excitations have been undertaken, and their effect on intensity of spectral density function has been investigated in presence of impurity and anharmonicity. The effect of force constant change parameter and atomic force constants has been undertaken to investigate the present property.

Keywords: *Electron, Phonon, Phonon - phonon interaction, Electron Green`s function, Electron phonon coupling constant, Semiconductor, Spectral density function,*

List of symbols used in equations:

1. π = pi
2. * = Star
3. α = alpha
4. β = beta
5. ε = epsilon
6. $\hbar$ = hcross
7. $\rightarrow$ = Arrow
8. ω = omega
9. Δ = delta
10. $\tilde{\varepsilon}_q$ = cap over ε_q
11. $\delta_{kk'}$ = Kronecker delta function
12. $\delta(\ )$ = Dirac delta function
13. $\tilde{n}_k$ = cap over n_k
14. θ = theta
15. η = eta
16. Γ = gamma
17. $\approx{n}_k$ = double cap over n_k
18. $\sum$ = summation

1. Introduction

The dynamics of the crystal is known by their dynamical constituents. The work on monolayer IV-VI semiconductors and magnetic semiconductors EuO (Averyanov et al., 2015: Liu et al., 2015) has been done by the researchers to promote the semiconductor technology. The different types of semiconductors such as diamond structure, zincblende structure, wurtzite structure are being applied in many fields. Real semiconductor crystals contain electron, phonon, impurity, and anharmonicity. In harmonic approximation, normal mode of vibrations are independent to one another and forces between atoms is a linear function of displacements (Callaway,1974). But in real crystal, the harmonic nature is destroyed in presence of impurity and anharmonicity. The presence of impurity creates localized mode

(Indu,1990). An anharmonicity can not be neglected even at 00K. An anharmonicity comes into an account by taking cubic and quartic terms beyond the quadratic term of Taylor series expansion of potential energy. This results in a formation of phonon-phonon interaction (Madelung,1978). In present case of semiconductor crystal, phonon- phonon interaction is taken to extract the information through excitations of electron. An electron moves in localized and anharmonic fields to create dynamical system in semiconductor crystals. An electron Green`s function is taken to investigate the study of spectral density function through electron phonon linewidth. This property is well understood by obtaining Fourier transformed electron Green`s function with the help of Hamiltonian.This type of Hamiltonian is contributed by harmonic part, electron part, electron phonon interaction part, defect part, and anharmonic part. This study is done on the basis of sections. These are formulation of the problem, evaluation of electron phonon linewidth, effect of phonon-phonon interaction on spectral density function, and conclusion of the work.

2. Formulation of the problem

Electron and phonon are the main constituents of semiconductor crystals. Spectral density *qq*function $J_{qq}(kqQ)$ is taken as (Zubarev, 1960: Pathak,1965)

$$J_{qq^{`}}(kqQ) = -2[\exp(\beta\hbar\varepsilon)+1]^{-1}\,\mathrm{Im}.G_{qq^{`}}(\varepsilon) \tag{1}$$

In eq.(1), Im.$G_{qq^{`}}$ (ε) indicates the imaginary part of Fourier transformed electron Green`s function *Gqq*(ε). This Fourier transformed electron Green`s function $G_{qq^{`}}$(ε) is to be obtained from equation of motion technique of quantum dynamics.

3. Evaluation of electron phonon linewidth

The Fourier transformed electron Green`s function can be evaluated with the help of many body approach. This approach is processed by taking Hamiltonian. This Hamiltonian H containsharmonic part H_{op},electron part H_{oe}, electron phonon interaction part H_{ep}, defect part H_D, and anharmonic part $H_A$as (Maradudin et al., 1971: Frohlich, 1966 : Fan, 1987 : Feinberg etal., 1990 : Mahanty and Behera, 1983 : Behera and Mishra, 1985 : Ziman, 1969 : Sharma and Bahadur, 1975 : Sahu and Sharma, 1983 : Pathak, 1965 : Indu, 1990).

$$H = H_{op} + H_{oe} + H_{ep} + H_D + H_A \tag{2}$$

Where,

$$H_{op} = \hbar/_4 \sum_k \varepsilon_k \left[A_k^* A_k + B_k^* B_k \right] \tag{3a}$$

$$H_{oe} = \hbar \sum_q \varepsilon_q b_q^* b_q \tag{3b}$$

$$H_{ep} = g\hbar \sum_{k,q} b_Q^* b_q B_k \tag{3c}$$

$$H_D = \hbar \sum_{k_1,k_2} \left[D(\vec{k}_1, \vec{k}_2) A_{k_1} A_{k_2} - C(\vec{k}_1, \vec{k}_2) B_{k_1} B_{k_2} \right] \tag{3d}$$

$$H_A = \hbar \sum_{s \geq 3} \sum_{k_1, k_2, \ldots, k_s} V^{(s)}(\vec{k}_1, \vec{k}_2, \ldots, \vec{k}_s) A_{k_1} A_{k_2} \cdots A_{k_s} \tag{3e}$$

where ,

$$A_k = a_k + a_{-k}^* = A_k^* \; ; B_k = a_k - a_{-k}^* = -B_{-k}^* \; ; \; \vec{Q} = \vec{k} + \vec{q} \tag{4}$$

The notations op, oe, ep, D, and A of eqs.(3a-3e) denote harmonic part, electron part, electron phonon interaction part, and anharmonic part of Hamiltonian respectively.

In eqs.(3a-3e), $b_q(b_q^*), a_k(a_k^*), \varepsilon_q, \varepsilon_k, g, D(\vec{k}_1, \vec{k}_2), C(\vec{k}_1, \vec{k}_2), V^{(s)}(\vec{k}_1, \vec{k}_2, \ldots, \vec{k}_s)$ are electron annihilation (creation) operators, phonon annihilation (creation) operators, electron band energy, phonon frequency(in energy unit), electron phonon coupling constant, force constant change parameter, mass change parameter, and Fourier transforms of atomic force constants respectively which are defined in references (Maradudin et al., 1971: Frohlich, 1966 : Fan, 1987 : Feinberg et al., 1990 : Mahanty and Behera, 1983 : Behera and Mishra, 1985 : Ziman,1969 : Sharma and Bahadur, 1975 : Sahu and Sharma,1983 : Pathak 1965: Indu, 1990). The Fourier transformed electron Green`s function $G_{qq'}(\varepsilon)$. can be obtained with the help of Hamiltonian eqs.(3a-3e) by applying equation of motion technique of quantum dynamics, and Dyson equation approach as(Zubarev,1960 : Sharma and Bahadur, 1975 : Sahu and Sharma, 1983 : Indu,1990 : Painuli et al., 1993 : Srivastava et al. 1996)

$$G_{qq'}(\varepsilon) = \left(\delta_{qq'} / \pi \right) \left[\left(\varepsilon - \tilde{\varepsilon}_q \right) + i\Gamma_{ep}(kqQ, \varepsilon) \right]^{-1} \tag{5}$$

In eq.(5), perturbed mode energy $\tilde{\varepsilon}_q$ is given as

$$\tilde{\varepsilon}_q = \varepsilon_q + \Delta_{ep}(kqQ, \varepsilon) \tag{6}$$

An electron phonon linewidth $\Gamma_{ep}(kqQ, \varepsilon)$ and electron phonon shift $\Delta_{ep}(kqQ, \varepsilon)$ of eq.(5) and eq.(6) are related through response function $P_{ep}(kqQ, \omega)$ as

$$P_{ep}(kqQ, \omega) = \Delta_{ep}(kqQ, \varepsilon) - i\Gamma_{ep}(kqQ, \varepsilon), \quad \omega \to 0^+ \tag{7}$$

This technique gives electron phonon linewidth $\Gamma_{ep}(kqQ, \varepsilon)$ as

$$\Gamma_{ep}(kqQ,\varepsilon)=\Gamma_{oep}(kqQ,\varepsilon)+\Gamma_{oep'}(kqQ,\varepsilon)+\Gamma_{oe}(kqQ,\varepsilon)+\Gamma_{D}(kqQ,\varepsilon)+\Gamma_{De}(kqQ,\varepsilon)+$$
$$\Gamma_{3A}(kqQ,\varepsilon)+\Gamma_{3Ae}(kqQ,\varepsilon)+\Gamma_{4A}(kq,\varepsilon)+\Gamma_{4Ae}(kq,\varepsilon) \quad (8)$$

Where,

$$\Gamma_{oep}(kqQ,\varepsilon)=4\pi g^2 N_Q\{\varepsilon_{+kq}{}^2 X_{kq}{}^2(+)\delta(\varepsilon+\varepsilon_k)-\varepsilon_{-kq}{}^2 X_{kq}{}^2(-)\delta(\varepsilon-\varepsilon_k)+2\varepsilon_q\varepsilon_k$$
$$(\varepsilon_k{}^2-3\varepsilon_q{}^2)(X_{kq}{}^2)^2\delta(\varepsilon-\varepsilon_q)\} \quad (9a)$$

$$\Gamma_{oep'}(kqQ,\varepsilon)=-\pi g^4\varepsilon_k\Bigg(4\varepsilon_q{}^2\tilde{\tilde{n}}_k+4\varepsilon_q\varepsilon_k\tilde{n}_k+\varepsilon_k{}^2 n_k+72\sum_{k_1,k_2}\left|V^{(3)}(\vec{k}_1,\vec{k}_2,-\vec{k})\right|^2 n_{k_1}n_{k_2}+384$$
$$\sum_{k_1,k_2,k_3}\left|V^{(4)}(\vec{k}_1,\vec{k}_2,\vec{k}_3-\vec{k})\right|^2\times n_{k_1}n_{k_2}n_{k_3}+16\sum_{k_1}\left|D(\vec{k}_1,-\vec{k})\right|^2 n_{k_1}\Bigg)\Big[4^{-1}\varepsilon_k{}^{-2}$$
$$X_{Q4k}{}^2\left\{\tfrac{5}{3}X_{2kq}{}^2(+)\,\delta(\varepsilon+2\varepsilon_k)-X_{2kq}{}^2(-)\,\delta(\varepsilon-2\varepsilon_k)\right\}-2^{-1}\varepsilon_k{}^{-2}$$
$$X_{Qk}{}^2\left\{X_{kq}{}^2(+)\,\delta(\varepsilon+\varepsilon_k)-X_{kq}{}^2(-)\delta(\varepsilon-\varepsilon_k)\right\}\Big] \quad (9b)$$

$$\Gamma_{oe}(kqQ,\varepsilon)=\pi g^2\Bigg(4\varepsilon_q{}^2\tilde{\tilde{n}}_k+4\varepsilon_q\varepsilon_k\tilde{n}_k+\varepsilon_k{}^2 n_k+72\sum_{k_1,k_2}\left|V^{(3)}(\vec{k}_1,\vec{k}_2,-\vec{k})\right|^2 n_{k_1}n_{k_2}+384$$
$$\sum_{k_1,k_2,k_3}\left|V^{(4)}(\vec{k}_1,\vec{k}_2,\vec{k}_3-\vec{k})\right|^2\times n_{k_1}n_{k_2}n_{k_3}+16\sum_{k_1}\left|D(\vec{k}_1,-\vec{k})\right|^2 n_{k_1}\Bigg)$$
$$(\varepsilon_q+\varepsilon_Q)^{-2}\left[\delta(\varepsilon-\varepsilon_q)-\delta(\varepsilon+\varepsilon_Q)\right] \quad (9c)$$

$$\Gamma_D(kqQ,\varepsilon)=16\pi g^2 N_Q\sum_{k_1}\left|D(\vec{k}_1,-\vec{k})\right|^2\left[X_{k_1q}{}^2(-)\delta(\varepsilon+\varepsilon_{k_1})-X_{k_1q}{}^2(+)\delta(\varepsilon-\varepsilon_{k_1})\right] \quad (9d)$$

$$\Gamma_{De}(kqQ,\varepsilon)=64\pi g^2 N_Q\varepsilon_q\sum_{k_1}\left|D(\vec{k}_1,-\vec{k})\right|^2\varepsilon_{k_1}(X_{k_1q}{}^2)^2\delta(\varepsilon-\varepsilon_q) \quad (9e)$$

$$\Gamma_{3A}(kqQ,\varepsilon)=36g^2 N_Q\sum_{k_1,k_2}\left|V^{(3)}(\vec{k}_1,\vec{k}_2,-\vec{k})\right|^2\eta_1\Big[S_{+1}\left\{X_{+\alpha q}{}^2(+)\delta(\varepsilon+\varepsilon_{+\alpha})-X_{+\alpha q}{}^2(-)\delta(\varepsilon-\varepsilon_{+\alpha})\right\}$$
$$+S_{-1}\left\{X_{-\alpha q}{}^2(+)\delta(\varepsilon+\varepsilon_{-\alpha})-X_{-\alpha q}{}^2(-)\delta(\varepsilon-\varepsilon_{-\alpha})\right\}\Big] \quad (9f)$$

$$\Gamma_{3Ae}(kqQ,\varepsilon)=144g^2 N_Q\varepsilon_q\sum_{k_1,k_2}\left|V^{(3)}(\vec{k}_1,\vec{k}_2,-\vec{k})\right|^2\eta_1\left(S_{+1}\varepsilon_{+\alpha}X_{+\alpha q}{}^2+S_{-1}\varepsilon_{-\alpha}X_{-\alpha q}{}^2\right)\delta(\varepsilon-\varepsilon_q) \quad (9g)$$

$$\Gamma_{4A}(kqQ,\varepsilon)=32g^2 N_Q\sum_{k_1,k_2,k_3}\left|V^{(4)}(\vec{k}_1,\vec{k}_2,\vec{k}_3-\vec{k})\right|^2\eta_2\Big[S_{+2}\left\{X_{+\beta q}{}^2(+)\delta(\varepsilon+\varepsilon_{+\beta})-X_{+\beta q}{}^2(-)\right.$$

$$\delta(\varepsilon-\varepsilon_{+\beta})\ \}+3S_{-2}\{X_{-\beta q}{}^{2}(+)\delta(\varepsilon+\varepsilon_{-\beta})-X_{-\beta q}{}^{2}(-)\delta(\varepsilon-\varepsilon_{-\beta})\ \}\ ] \qquad (9h)$$

$$\Gamma_{4Ae}(kqQ,\varepsilon)=128g^{2}N_{Q}\varepsilon_{q}\sum_{k_1,k_2,k_3}\left|V^{(4)}(\vec{k}_1,\vec{k}_2,\vec{k}_3,-\vec{k})\right|^{2}\eta_{2}\left(S_{+2}\varepsilon_{+\beta}X_{+\beta q}{}^{2}+3S_{-2}\varepsilon_{-\beta}X_{-\beta q}{}^{2}\right)\delta(\varepsilon-\varepsilon_{q}) \qquad (9i)$$

The various symbols in above eqs.(9a-9i) are given in the following equations as

$$\tilde{n}_k=\langle A_k B_k\rangle\ ;\ \overset{\approx}{n}_k=\langle B_k{}^{*}B_k\rangle\ ;\ n_k=\langle A_k{}^{*}A_k\rangle\ ;\ \varepsilon_{\pm\alpha}=\tilde{\varepsilon}_{k_1}\pm\tilde{\varepsilon}_{k_2}\ ;\ \ \varepsilon_{\pm\beta}=\tilde{\varepsilon}_{k_1}\pm\tilde{\varepsilon}_{k_2}\pm\varepsilon_{k_3}\ ;$$

$$\varepsilon_{\pm kq}{}^{2}=\varepsilon_{k}{}^{2}-\varepsilon_{q}{}^{2}\pm\varepsilon_{q}\varepsilon_{k} \qquad (10a)$$

$$N_{Q}=\langle b_{Q}{}^{*}b_{Q}\rangle\ ;n_{k}=\left(\tilde{\varepsilon}_{k}/\varepsilon_{k}\right)Coth\left(\beta\hbar\varepsilon_{k}/2\right) \qquad (10b)$$

$$S_{\pm1}=n_{k_2}\pm n_{k_1}\ \ ;\ \ S_{\pm2}=1\pm n_{k_1}n_{k_2}+n_{k_2}n_{k_3}\pm n_{k_3}n_{k_1} \qquad (10c)$$

$$\eta_{i-1}=\varepsilon_{k_1}\varepsilon_{k_2}\ldots\varepsilon_{k_i}\Big/\tilde{\varepsilon}_{k_1}\tilde{\varepsilon}_{k_2}\ldots\tilde{\varepsilon}_{k_i}\ \ :\ X_{ij}{}^{2}(\pm)=1\Big/(\varepsilon_{i}\pm n'\varepsilon_{j})^{2}\ ;n'=1,2\ ;\ i=k,k_1,\pm\alpha,\pm\beta\ ;\ j=q\ :$$

$$X_{lm}{}^{2}=1\Big/(\varepsilon_{l}{}^{2}-n''\varepsilon_{m}{}^{2})\ \ ;\ n''=1,4\ \ ;\ l=k,k_1,\pm\alpha,\pm\beta,Q\ \ ;\ \ m=k,q \qquad (10d)$$

An electron phonon linewidth of eq.(8) represented by (oep ,oep`) ,(D,De), (3A,3Ae), and (4A,4Ae) are contributed by interaction of electron with harmonic field , localized field, cubic anharmonic field and quartic anharmonic field respectively.

4. Effect of Phonon-phonon Interaction on Spectral Density Function

The spectral density function $J_{qq'}(kqQ)$ can be obtained by substitution of imaginary part of eq.(5) into eq.(1) through eqs.(9a-9i) as(Painuli et al.,1993: Srivastava et al.,1996)

$$J_{qq'}(kqQ)=J_{qq'}{}^{oep}(kqQ)+J_{qq'}{}^{oep'}(kqQ)+J_{qq'}{}^{oe}(kqQ)+J_{qq'}{}^{D}(kqQ)+J_{qq'}{}^{De}(kqQ)$$
$$+J_{qq'}{}^{3A}(kqQ)+J_{qq'}{}^{3Ae}(kqQ)+J_{qq'}{}^{4A}(kqQ)+J_{qq'}{}^{4Ae}(kqQ) \qquad (11)$$

Each terms of eq.(11) are given as

$$J_{qq'}{}^{oep}(kqQ)=8g^{2}k_{B}\hbar^{-1}N_{Q}TX_{eq}\{\varepsilon_{+kq}{}^{2}X_{kq}{}^{2}(+)\delta(\varepsilon+\varepsilon_{k})-\varepsilon_{-kq}{}^{2}X_{kq}{}^{2}(-)\delta(\varepsilon-\varepsilon_{k})+2\varepsilon_{q}\varepsilon_{k}$$
$$(\varepsilon_{k}{}^{2}-3\varepsilon_{q}{}^{2})(X_{kq}{}^{2})^{2}\delta(\varepsilon-\varepsilon_{q})\ \} \qquad (12a)$$

$$J_{qq'}{}^{oep'}(kqQ)=-2g^{4}k_{B}\hbar^{-1}T\varepsilon_{k}X_{eq}\Bigg(4\varepsilon_{q}{}^{2}\overset{\approx}{n}_{k}+4\varepsilon_{q}\varepsilon_{k}\tilde{n}_{k}+\varepsilon_{k}{}^{2}n_{k}+72\sum_{k_1,k_2}\left|V^{(3)}(\vec{k}_1,\vec{k}_2,-\vec{k})\right|^{2}n_{k_1}n_{k_2}+$$
$$384\sum_{k_1,k_2,k_3}\left|V^{(4)}(\vec{k}_1,\vec{k}_2,\vec{k}_3-\vec{k})\right|^{2}\times n_{k_1}n_{k_2}n_{k_3}+16\sum_{k_1}\left|D(\vec{k}_1,-\vec{k})\right|^{2}n_{k_1}\Bigg)\Big[4^{-1}\varepsilon_{k}{}^{-2}X_{Q4k}{}^{2}$$
$$\{5/3\,X_{2kq}{}^{2}(+)\delta(\varepsilon+2\varepsilon_{k})-X_{2kq}{}^{2}(-)\delta(\varepsilon-2\varepsilon_{k})\}-2^{-1}\varepsilon_{k}{}^{-2}X_{Qk}{}^{2}$$

$$\left\{X_{kq}{}^{2}(+)\delta(\varepsilon+\varepsilon_k)-X_{kq}{}^{2}(-)\delta(\varepsilon-\varepsilon_k)\right\}\Big] \quad (12b)$$

$$J_{qq'}{}^{ae}(kqQ) = 2g^2k_B\hbar^{-1}T\Big(4\varepsilon_q{}^2\tilde{\tilde{n}}_k+4\varepsilon_q\varepsilon_k\tilde{n}_k+\varepsilon_k{}^2n_k+72\sum_{k_1,k_2}\left|V^{(3)}(\vec{k}_1,\vec{k}_2,-\vec{k})\right|^2n_{k_1}n_{k_2}+384$$

$$\sum_{k_1,k_2,k_3}\left|V^{(4)}(\vec{k}_1,\vec{k}_2,\vec{k}_3-\vec{k})\right|^2n_{k_1}n_{k_2}n_{k_3}+16\sum_{k_1}\left|D(\vec{k}_1,-\vec{k})\right|^2n_{k_1}\Big)(\varepsilon_q+\varepsilon_Q)^{-2}$$

$$X_{\varepsilon q}\left[\delta(\varepsilon-\varepsilon_q)-\delta(\varepsilon+\varepsilon_Q)\right] \quad (12c)$$

$$J_{qq'}{}^{D}(kqQ)=32g^2k_B\hbar^{-1}TN_Q\sum_{k_1}\left|D(\vec{k}_1,-\vec{k})\right|^2X_{\varepsilon q}[\ X_{k_1q}{}^2(-)\delta(\varepsilon+\varepsilon_{k_1})-X_{k_1q}{}^2(+)\delta(\varepsilon-\varepsilon_{k_1})\ ] \quad (12d)$$

$$J_{qq'}{}^{De}(kqQ)=128g^2k_B\hbar^{-1}TN_Q\varepsilon_q\sum_{k_1}\left|D(\vec{k}_1,-\vec{k})\right|^2\varepsilon_{k_1}X_{\varepsilon q}(X_{k_1q}{}^2)^2\delta(\varepsilon-\varepsilon_q) \quad (12e)$$

$$J_{qq'}{}^{3A}(kqQ)=72g^2N_Q\pi^{-1}\hbar^{-2}k_B{}^2T^2\sum_{k_1,k_2}\left|V^{(3)}(\vec{k}_1,\vec{k}_2,-\vec{k})\right|^2(\varepsilon_{k_1}{}^{-1}+\varepsilon_{k_2}{}^{-1})X_{\varepsilon q}\eta_1\big[X_{+\alpha q}{}^2(+)$$

$$\delta(\varepsilon+\varepsilon_{+\alpha})-X_{+\alpha q}{}^2(-)\delta(\varepsilon-\varepsilon_{+\alpha})\big] \quad (12f)$$

$$J_{qq'}{}^{3Ae}(kqQ)=288g^2\varepsilon_qN_Q\pi^{-1}\hbar^{-2}k_B{}^2T^2\sum_{k_1,k_2}\left|V^{(3)}(\vec{k}_1,\vec{k}_2,-\vec{k})\right|^2\eta_1\varepsilon_{+\alpha}X_{+\alpha q}{}^2(\varepsilon_{k_1}{}^{-1}+\varepsilon_{k_2}{}^{-1})X_{\varepsilon q}\delta(\varepsilon-\varepsilon_q)$$

$$(12g)$$

$$J_{qq'}{}^{4A}(kqQ)=64g^2N_Q\pi^{-1}\hbar^{-3}k_B{}^3T^3\sum_{k_1,k_2,k_3}\left|V^{(4)}(\vec{k}_1,\vec{k}_2,\vec{k}_3-\vec{k})\right|^2(\varepsilon_{k_1}{}^{-1}\varepsilon_{k_2}{}^{-1}+\varepsilon_{k_2}{}^{-1}\varepsilon_{k_3}{}^{-1}+\varepsilon_{k_3}{}^{-1}\varepsilon_{k_1}{}^{-1})$$

$$X_{\varepsilon q}\eta_2\left[X_{+\beta q}{}^2(+)\delta(\varepsilon+\varepsilon_{+\beta})-X_{+\beta q}{}^2(-)\ \delta(\varepsilon-\varepsilon_{+\beta})\right] \quad (12h)$$

$$J_{qq'}{}^{4Ae}(kqQ)=256g^2\varepsilon_qN_Q\pi^{-1}\hbar^{-3}k_B{}^3T^3\sum_{k_1,k_2,k_3}\left|V^{(4)}(\vec{k}_1,\vec{k}_2,\vec{k}_3-\vec{k})\right|^2\eta_2\varepsilon_{+\beta}X_{+\beta q}{}^2(\varepsilon_{k_1}{}^{-1}\varepsilon_{k_2}{}^{-1}+\varepsilon_{k_2}{}^{-1}\varepsilon_{k_3}{}^{-1}$$

$$+\varepsilon_{k_3}{}^{-1}\varepsilon_{k_1}{}^{-1})X_{\varepsilon q}\delta(\varepsilon-\varepsilon_q) \quad (12i)$$

where,

$$X_{\varepsilon q}=\left\{\varepsilon(\varepsilon^2-\tilde{\varepsilon}_q{}^2)^2\right\}^{-1} \quad (13)$$

5. Conclusion

The present study is based on different interactions as of electron with harmonic, localized and anharmonic fields. This many body approach based on electron Green`s function gives various contributions to spectral density function. It is found that cubic and quartic anharmonic parts are depended as T^2 and T^3 on temperature in comparison to T dependence on temperature due to harmonic part, electron part, and defect part. One phonon bound state, two phonon bound state, exciton state are found in harmonic field, exciton state, polaron state are found in electron electronfield, two phonon combination and difference bands $\varepsilon_{\pm\alpha}$, exciton state are found in cubicanharmonic field, three phonon combination and difference bands $\varepsilon_{\pm\alpha}$, exciton state are occurred in quartic anharmonic field. When one phonon bound state, two phonon state, localized state, two and three phonon combination and difference bands are approached to the exciton state, the intensity of peaks of perturbed spectrum increases asymptotically. It is also known that threephonons and four phonons are participated to form a exciton. The presence of N_Q in each term is the birth of polaron besides electron electron interaction part. The non linear dependence on electron phonon coupling constant, force constant change parameter, atomic force constants are the factors which greatly influenced this property. The non-linear dependence on electron phonon coupling constant of delta function peaks shows that in semiconductor crystal this type of response only due to electron phonon interaction. It is concluded that if creation of exciton state is due to destruction of polaron state, then electron electron interaction field contributes significantly for spectral density function. When frequency becomes identical with perturbed mode energy, spectral density function shows sharper peaks of excitations namely harmonic phonon, localized phonon, exciton, polaron, combination, and difference bands.The study of spectral density function will help in explaining the different physical properties of semiconductor crystal particularly optical related properties.

References

- *A. A. Maradudin, E. W. Montroll, G. H. Weiss, and I. P. Ipatova, (1971), Solid State Physics, Supplement 3, Theory of Lattice Dynamics in the Harmonic Approximation 2nd edition, Academic Press, New York , London, ch.2, 56.*
- *Averyanov Dmitry V., Teterin Peter E., Sadofyev Yuri G., Likhachev Igor A., Primenko Alexey E., Tokma Chev Andrey M., and Storchak Vyachslav G., 2015, Epitaxial Growth of Magnetic Semiconductor EuO on Silicon By Molecular Beam Epitaxy, Crystal Research and Technology, 50(3), 268-275[DOI: 10.1002/crat201500005].*
- *Behera S. N., and Mishra S. G., 1985, Electron - Phonon Interaction in Charge – density - wave Superconductors, Physical Review B, 31(5), pp 2773-2775.*
- *Feinberg D.,Ciuchi S., and dePasquale F.,1990,Squeezing Phenomena in Interacting Electron– Phonon Systems, International Journal of Modern Physics B,4(7 & 8), pp 1317-1367.*
- *Frohlich H.(1966), New Perspectives In Modern Physics, Ed. R. E. Marshak, John Wiley & Sons, New York ,539.*
- *H. Y. Fan,(1987), Elements of Solid State Physics, John Wiley & Sons, New York, 183&184.*
- *Indu B. D., 1990, Theory of Lattice Specific Heat of an Isotopically Disordered Anharmonic Crystal, International Journal of Modern Physics B, 4(7 & 8), pp 1379-1393.*
- *J. Callaway(1974), Quantum Theory of the Solid State (Part A), Academic Press, New York, London, ch.1,1.*
- *J. M. Ziman, (1969), Elements of Advanced Quantum Theory, Cambridge University Press, Cambridge, ch. 2, 38 & 43.*
- *Liu Junwei, Qian Xiaofeng, and Fu Liang, 2015, Crystal Field Effect Induced Topological Crystalline Insulators In Monolayer IV-VI Semiconductors, Nano Letters,15(4), 2657-2661 [10.1021/acs. nanolett .5b00308].*
- *Mahanty G. C., and Behera S. N., 1983, Dispersion of Superconducting Gap Excitations in Layered Charge Density Wave Systems, Canadian Journal of Physics, 61(8), pp 1160-1168.*
- *O. Madelung , (1978), Introduction to Solid-State theory, Springer Series in Solid-State Sciences ; Vol. 2 , Translated by B. C. Taylor ,Eds. Manuel Cardona , Peter Fulde , Hans-Joachim Queisser, Springer-Verlag Berlin Heidelberg, ch.3 and Ch. 7.*
- *Painuli C.P., Chandra Jagdish, and Indu B.D., 1993, Infrared Absorption in Defect Induced Anharmonic Solids, Pramana Journal of Physics, 40(5), pp 345-356.*
- *Pathak K. N., 1965, Theory of Anharmonic Crystals, Physical Review,139(5A), pp A1569-A1580.*
- *Sahu D. N., and Sharma P. K., 1983, Thermal Conductivity of an Imperfect Anharmonic Crystal, Physical Review B, 28(6), pp 3200-3213.*
- *Sharma P. K., and Bahadur R., 1975, Thermal Conductivity for Phonon Scattering by Substitutional Defects in Crystals, Physical Review B, 12(4), pp 1522-1530.*
- *Srivastava S., Raiwani Y.P., Gairola S.C., and Indu B. D., 1996, Electrons in Anharmonic Phonon Fields of Low-dimensional High-T_c Superconductors, Physica B, 223 & 224, pp 538-540.*
- *Zubarev D. N., 1960, Double-Time Green Functions in Statistical Physics, Usp. Fiz. Nauk, 71, pp 71- 116 [Eng. Transl. Soviet Physics Uspekhi, 1960, 3(3), pp 320-345].*

Optimizing and Predicting Surface Roughness on Milling Machine By Using Taguchi & Ann on D2 Steel

Er. Alamdeep Cheema*, Er. Rajiv Kumar**

**Post Graduate student in Industrial and Production Engineering at GIMT, Kurukshetra.*

*** Assistant Professor in Mechanical engineering department at GIMT, Kurukshetra.*

ABSTRACT

Optimization means to find best value of input. For this Taguchi method gives the best output result. ANOVA is the most effecting parameter. This parameter affects the most among all the input parameters. Modeling is done by ANN. It is best network model which gives minimum error between network output and real output. Prediction is done by both methods. Result of both methods is compared. Best method is used which gives the minimum error. Milling process is used here because milling is most commonly used in industries. It can perform many tasks. D2 steel is used here. Various parameter are considered in this are taken from the previous papers. Taguchi and ANN methods are used because these are the most famous and developing methods. Taguchi method is used for optimization. It is done by studying the mathematical relation between input and output. Signal to noise ratio is basically considered in the optimization process. Signal should be large and noise should be less. ANN method is used for prediction. It shows that for any value of input data we can easily predict the output with minimum error.

Keywords: *Milling machining, D2 steel, surface roughness, Taguchi, ANOVA, ANN etc.*

I. INTRODUCTION

Recent functionality requirements have led to development of components with varying free-form features. Sculptured surfaces have free-form features with both convex and concave regions that can be geometrically fitted by ball-end cutter. The parts with free from geometric features are generally machined using ball-end cutters, which are used to manufacture parts in die/mould, aerospace, biomedical and automotive industries where both part quality and manufacturing time are metrics for high productivity. The ultimate goal of virtual machining process research is to identify process related issues and solve them before the costly physical trials in the shop. Modeling the process mathematically is necessary to achieve that goal in a Reasonable amount of time and the first step of process modeling is to model the mechanics of the operation that leads to the prediction of the cutting forces experienced by the cutting tool and the work-piece.

2. LITERATURE REVIEW

R. Peres et.al. (1999) proposed that process optimization is a very important subject to several industrial sectors in confronting the growth on markets competition. However, due to the complexity of some processes, their optimization is not an easy task; therefore, to accomplish this objective, intelligent techniques should be used. We are working on end-milling process optimization through combining analytic and fuzzy techniques.

J. F. Briceno et.al. (2002) proposed that two supervised neural networks are used to estimate the forces developed during milling. These two Artificial Neural Networks (ANNs) are compared based on a cost function that relates the size of the training data to the accuracy of the model.

H. E. Mounayri et.al. (2005) proposed an integrated product development system for optimized CNC ball end milling is presented. First, the developed model is extended from flat end milling to ball end milling. Second, the optimization is extended from 2D (speed and feed) to 3 (1/2) D (speed, feed, radial and axial depths of cut).

K.Kadirgama et.al. (2008) is concerned with optimization of the surface roughness when milling Mould Aluminum alloys (AA6061-T6) with carbide coated inserts. Optimization of milling is very useful to reduce cost and time for machining mould. The approach is based on Response Surface Method (RSM) and Radian Basis Function Network (RBFN).

S.Brevern et.al. (2009) proposed that the world of manufacturing has shifted its level to the era of space age machining. The purpose of this investigation is to develop Fuzzy based Graphical User Interface (GUI) for modeling of laser machining conditions.

M.S. Yazdi et.al. (2010) studied that the selection of optimal machining parameters (i.e., spindle speed, depth of cut and feed rate) for face milling operations was investigated in order to minimize the surface roughness and to maximize the material removal rate. Effects of selected parameters on process variables (i.e., surface roughness and material removal rate) were investigated using Response Surface Methodology (RSM) and artificial neural networks.

S.Moshat et.al. (2010) proposed that End milling is the most important milling operation, widely used in most of the manufacturing industries due to its capability of producing complex geometric surfaces with reasonable accuracy and surface finish. However, with the inventions of CNC milling machine, the flexibility has been adopted along with versatility in end milling process.

B. S.Reddy et.al. (2011) proposed that Pre-hardened steel (P20) is a widely used material in the production of moulds/dies due to less wear resistance and used for large components. In this study, minimization of surface roughness has been investigated by integrating design of experiment method, Response surface methodology (RSM) and genetic algorithm.

A. K.Gupta et.al. (2011) proposed that the optimum combination of machining parameters has been analyzed for maximizing the tool life with the constraints of material removal rate (MRR) and surface finish. To optimize these parameters the correct relationship of process parameters with tool life has been found. Mathematical relations have been developed for predicting the objectives with different combinations of parameters under the specified constraints. As there is a variety of milling processes, cutting tool geometries, cutting tool material, work piece material and machine tool conditions, hence difficult to develop a single robust analytical relation for tool life.

P.Maurya et.al. (2012) studied on CNC end milling, influence of various machining parameters like, tool feed (mm/min),tool speed (rpm), tool diameter (mm) and depth of cut (mm). In the present study, experiments are conducted on AL 6351 –T6material with three levels and four factors to optimize process parameter and surface roughness

S. Hossain et. al. (2012) proposed that Surface roughness is an index which determines the quality of machined products and is influenced by the cutting parameters. In this study the average surface roughness (Ra) value for Aluminum after ball end milling operation has been measured. 84 experiments have been conducted varying cutter axis inclination angle (φ degree), spindle speed (S rpm), feed rate (mm/min), radial depth of cut (feed f mm), and axial depth of cut (t mm) in order to find Ra. This data has been divided into two sets on a random basis; 68 training data set and 16 testing data set.

A.Behera et. al. (2012) proposed that Plasma spraying technique has become a subject of intense research in many industrial structural/functional applications because its peculiarity surface properties. This investigation explains about plasma sprayed copper surface property. Here industrial waste and low grade ore (i.e. Flay-ash+ quartz+ limonite), used as deposit material which is to be coated on copper substrates. In many applications, it is found that for structural modification, surface roughness & porosity parameters are very important. To decrease both surface roughness and coating porosity by optimizing other necessary properties, different soft computing methods like Artificial Neural Network (ANN) and Least Square support vector machine techniques used.

III. EXPERIMENTAL DETAILS

End Milling

Among different types of milling processes, end milling is one of the most vital and common metal cutting operations used for machining parts because of its capability to remove materials at faster rate with a reasonably good surface quality. Also, it is capable of producing a variety of configurations using milling cutter. In end milling, the cutter, called end mill, has a diameter less than the work piece width. The end mill has helical cutting edges carried over onto the cylindrical cutter surface. End mills with flat ends (so called squire-end mills) are used to produce pockets, closed or end key slots, etc.

In end milling an end mill makes either peripheral or slot cuts, determined by the step-over distance, across the work piece in order to machine a specified feature such as a profile, slot, pocket, or even a complex surface contour. The depth of the feature may be machined in a single pass or may be reached by machining at a smaller axial depth of cut and making multiple passes.

Material Used

In this work hardened AISI D2 steel (hardness 50-70 HRC) will be used as the work piece material and Tungsten carbide preferably coated will be used as the tool material. Because increasing tool life is main concern of hard machining to decrease the cost of the machining process. A particular amount of maximum flank wear say 0.2 to 0.3 μm can be used as the tool life failure criterion. Flank wear can be measured using toolmaker's microscope. The chemical composition of AISI D2 tool steel is given in below Table 3.1.

Table 3.1 Chemical Composition of Steel

Carbon	Silicon	Manganese	Chromium	Molybdenum	Vanadium
1.55%	0.30%	0.35%	12%	0.75%	0.90%

AISI D2 is recommended for tools requiring very high wear resistance, combined with moderate toughness (shock-resistance). AISI D2 can be supplied in various finishes, including the hot-rolled, pre-machined and fine machined condition forming Dies, Punches, Forming Rolls, Knives, Slitters, Shear blades.

Machine Used

Machining was carried out in CNC machine at CTR, Ludhiana.

Figure 1. CNC Milling Machine

Table 3.2 Specification of CNC Milling Machine

Table Size	915 * 356 mm
Table Load	341 KG
Power	3 phase, 60 Hz
Control	GE FANUC 211
X Axis Travel	560 mm
Y Axis Travel	406 mm
Z Axis Travel	508 mm
Spindle Speed	100 RPM Direct Drive
Spindle Diameter	65 mm
Spindle Taper	ISO-40
Tool Taper	BT-40
Magazine Capacity	22 Tools
Maximum Wt. of Tool Holder	50 KG
Maximum Tool Length	254

Table 3.3 Levels of Input Control Parameters

Factors	*Levels*	*Factor Level values*
Speed (rpm)	3	5,007,501,000
Depth of Cut (mm)	3	0.75,0.50,0.25
Feed (mm/min)	3	75,010,001,250

The optimum condition is identified by studying the main effects of each of the parameters. The main effects indicate the general trend of influence of each parameter. The knowledge of contribution of individual parameters is a key in deciding the nature of control to be established on a production process. Orthogonal Array is a statistical method of defining parameters that converts test areas into factors and levels. Test design using orthogonal array creates an efficient and concise test suite with fewer test cases without compromising test coverage. An orthogonal array is a "table" (array) whose entries come from a fixed finite set of symbols (typically, {1,2,..., n}), arranged in such a way that there is an integer t so that for every selection of t columns of the table, all ordered t-tuples of the symbols, formed by taking the entries in each row restricted to these columns, appear the same number of times. The number t is called the strength of the orthogonal array. The Table 3.4 shows the design matrix used in this work.

Table 3.4 Orthogonal Array L9

Sample No.	**Spindle Speed (rpm)**	**Feed Rate (mm/min.)**	**Depth Of Cut (mm)**
1	1	1	1
2	1	2	2
3	1	3	3
4	2	1	2
5	2	2	3
6	2	3	1
7	3	1	3
8	3	2	1
9	3	3	2

IV. EXPERIMENTAL PROCEDURES

- Checking and preparing the Centre Lathe ready for performing the machining operation.
- Firstly, the work-piece was cut according to above mentioned dimension i.e. 100*100*25 mm by cutter of diameter 32 mm.
- For developing models on the basis of experimental data three main machining parameters are considered to predict surface roughness of D2 material using carbide tool. Among the range of

spindle speed, feed, and depth of cut available possible in the machine the following three levels are considered as shown in Table 3.3.

- The machining was carried out on end milling machine, the material work piece is clamped on vice mounted on the table of the machine. The machining process and work tool motion of the end milling process respectively.
- The machining is carried out by selecting proper spindle speed and feed rate during each experimentation. Experiment was carried out by varying the depth of cut.

Taguchi's designs aimed to allow greater understanding of variation than did many of the traditional designs. Taguchi contended that conventional sampling is inadequate here as there is no way of obtaining a random sample of future conditions. Taguchi suggests a three-stage process:

- System design,
- Parameter design,
- Tolerance design.

System design is the conceptualization and synthesis of a product or process to be used. In parameter design the system variables are experimentally analyzed to determine how the product or process reacts to uncontrollable “noise” in the system; parameter design is the main thrust of Taguchi's approach. The final step in Taguchi's robust design approach is tolerance design; tolerance design occurs when the tolerances for the products or process are established to minimize the sum of the manufacturing and lifetime costs of the product or process.

Taguchi proposed extending each experiment with an "outer array" or orthogonal array should simulate the random environment in which the experiment would function. Here we use L9 orthogonal array with 3 levels. In this work, L9 Orthogonal Array design matrix is used to set the control parameters to evaluate the process performance. Taguchi orthogonal array is designed with three levels of turning parameters with the help of software Minitab. Orthogonal Array design of experiment has been found suitable in the present work.

V. RESULTS AND DISCUSSION

End milling is one of the most fundamental and commonly encountered chip removal operations occurring in a real manufacturing environment. In this machining process, the surface finish is a key factor in evaluating and determining the quality of a part. In practice, a desired surface roughness value is usually designated, and the appropriate cutting parameters are selected to achieve the desired quality of a specified part. The single point incremental forming (SPIF) process is performed on three-axis CNC machine.

Table 5.1 Measured Surface Roughness

Pieces	*Speed (rpm)*	*Depth of Cut (mm)*	*Feed (mm/min)*	*Surface Roughness (µm)*
1	*500*	*750*	*0.75*	*0.73*
2	*500*	*1000*	*0.50*	*0.77*
3	*500*	*1250*	*0.25*	*0.82*
4	*750*	*750*	*0.50*	*0.72*
5	*750*	*1000*	*0.25*	*0.49*
6	*750*	*1250*	*0.75*	*0.63*
7	*1000*	*750*	*0.25*	*0.42*
8	*1000*	*1000*	*0.75*	*0.72*
9	*1000*	*1250*	*0.50*	*0.55*

Table 5.2 Measured Roughness Parameters

Pieces	*R_a (µm)*	*R_t (µm)*	*R_z (µm)*	*R_c (µm)*
1	*0.73*	*3.94*	*2.97*	*1,91*
2	*0.77*	*4.22*	*3,34*	*2.45*
3	*0.82*	*4.46*	*3.62*	*2.88*
4	*0.72*	*3.87*	*2.94*	*1.87*
5	*0.49*	*2.14*	*1.82*	*1.21*
6	*0.63*	*3.41*	*2.69*	*1.64*
7	*0.42*	*2.02*	*1.71*	*1.16*
8	*0.72*	*3.89*	*2.95*	*1.88*
9	*0.55*	*2.87*	*1.98*	*1.34*

The main objective of the thesis is to optimize the milling parameters (spindle speed, feed rate, depth of cut and cutting tool grade) to achieve low value of the surface roughness. The experimental data for the surface roughness values is shown in Table 5.1.

6.1.2 Optimization by Taguchi Method

Since 1960, Taguchi methods have been used for improving the quality of Japanese products with great success. During the 1980's, many companies finally realized that the old methods for ensuring quality were not competitive with the Japanese methods. Performance characteristics are first converted into the S/N ratio using the Taguchi method. Using S/N quantity, optimal performance and minimal variance be designed. The SR value is calculated for each trial from the basic data collected . The signal to- noise ratios of each experimental run are calculated based on the following equation, which are listed in corresponding tables with the data.

$$SNR = -10log\frac{1}{n} \quad y^2$$

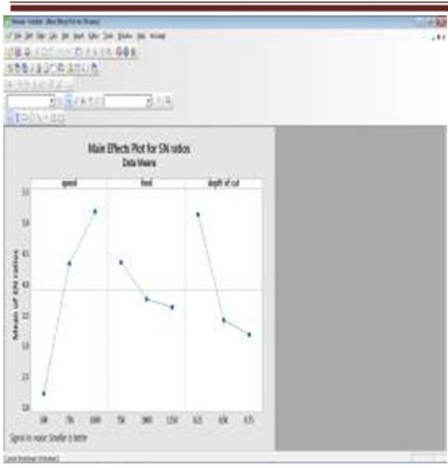

Analysis of Variance

Source	DF	Seq SS	Contribution	Adj SS	Adj MS	F-Value	P-Value
speed	2	13.8738	44.60%	13.8738	6.9369	1.46	0.407
feed	2	0.9118	2.93%	0.9118	0.4559	0.10	0.913
depth of cut	2	6.7995	21.86%	6.7995	3.3997	0.71	0.583
Error	2	9.5201	30.61%	9.5201	4.7600		
Total	8	31.1052	100.00%				

Figure 2-S/N ratio **Table 5.3 ANOVA**

Table 5.4 Comparison of Taguchi and ANN

Output Comparison of Taguchi Method and ANN Technique

Pieces	*SR*	*PSR (Taguchi)*	*Error (Taguchi)*	*Output (ANN)*	*Error (ANN)*
1	*0.73*	*0.79*	*0.06*	*0.73*	*0*
2	*0.77*	*0.81*	*0.04*	*0.77*	*0*
3	*0.82*	*0.71*	*-0.11*	*0.75*	*-0.07*
4	*0.72*	*0.61*	*-0.11*	*0.62*	*-0.1*
5	*0.49*	*0.55*	*0.06*	*0.49*	*0*
6	*0.63*	*0.67*	*0.04*	*0.63*	*0*
7	*0.42*	*0.46*	*0.04*	*0.42*	*0*
8	*0.72*	*0.61*	*-0.11*	*0.72*	*0*
9	*0.55*	*0.61*	*0.06*	*0.55*	*0*

VI. CONCLUSION

1. The higher the cutting speed, the lower is the surface roughness.
2. The experimental results show that average surface roughness is low at lower depth of cut.

3. For achieving good surface finish on the D2 work piece, higher cutting speed, lower feed and lower depth of cut are preferred. The optimal parametric combination for AISI D2 Steel is speed3-feed1- depth of cut1.
4. ANOVA shows that the cutting speed is the most influencing parameter for surface roughness.
5. Mean Absolute Percentage Error is calculated in Taguchi method is 10.77% and Mean Absolute Percentage is Calculated in MATLAB is 2.90% so ANN technique gives us better results than Taguchi method .Error is minimized by ANN technique.
6. Best Model achieved in ANN is with feed forwarded back propagation neural network with Levenberg-Marquardt training function with three layers.

VII. REFERENCES

1. *A.Behera, S.Behera, R.K Tripathy, S.C Mishra, "Least Square Support Vector Machine Alternative To Artificial Neural Network For Prediction Of Surface Roughness And Porosity Of Plasma Sprayed Copper Substrates", December, 2012.*
2. *A.Jameel, M. Minhat, Md. Nizam, "Using Genetic Algorithm to Optimize Machining Parameters in Turning Operation: A review", Volume 3, Issue 5, May 2013.*
3. *A.Joshi & P.Kothiyal, "Investigating Effect of Machining Parameters of CNC Milling on Surface Finish by Taguchi Method", Volume-2, Issue-2, 2013.*
4. *A.K Sahoo, "Application of Taguchi and regression analysis on surface roughness in machining hardened AISI D2 steel", International Journal of Industrial Engineering Computations 2014.*
5. *A.K Gupta, P.Chandna, P.Tandon, "Tool Life Optimization in 2.5d Milling By Coupling Regression Model And Genetic Algorithm", International Journal of Engineering and Technology Volume 1 No. 1, October, 2011.*
6. *A. Aggarwal and H. Singh, "Optimization Of Machining Techniques – A Retrospective and Literature Review" SadhanaVol. 30, Part 6, December 2005.*
7. *B.C Routara, S.D Mohanty, S.Datta, A. Bandyopadhyay and S.SMahapatra, "Optimization in CNC end milling of UNS C34000 medium leaded brass with multiple surface roughness characteristics," Vol. 35, Part 5, October 2010.*

AUTHORS BIOGRAPHIES

ALAMDEEP CHEEMA Passed his diploma in Mechanical engineering In 2008 from haryana state board of technical education and B.tech In 2008 From kurukshetra universitsy kurukshetra and pursuing M.tech from kuk.

RAJIV KUMAR passed his B.tech from JIET, jind in 2005 and M.tech from GJU Hisar in 2010. Presently he is working as the Assistant Professor in GIMT kurukshetra.

Instructions for Authors

Essentials for Publishing in this Journal

1 Submitted articles should not have been previously published or be currently under consideration for publication elsewhere.

2 Conference papers may only be submitted if the paper has been completely re-written (taken to mean more than 50%) and the author has cleared any necessary permission with the copyright owner if it has been previously copyrighted.

3 All our articles are refereed through a double-blind process.

4 All authors must declare they have read and agreed to the content of the submitted article and must sign a declaration correspond to the originality of the article.

Submission Process

All articles for this journal must be submitted using our online submissions system. http://enrichedpub.com/ . Please use the Submit Your Article link in the Author Service area.

Manuscript Guidelines

The instructions to authors about the article preparation for publication in the Manuscripts are submitted online, through the e-Ur (Electronic editing) system, developed by **Enriched Publications Pvt. Ltd**. The article should contain the abstract with keywords, introduction, body, conclusion, references and the summary in English language (without heading and subheading enumeration). The article length should not exceed 16 pages of A4 paper format.

Title

The title should be informative. It is in both Journal's and author's best interest to use terms suitable. For indexing and word search. If there are no such terms in the title, the author is strongly advised to add a subtitle. The title should be given in English as well. The titles precede the abstract and the summary in an appropriate language.

Letterhead Title

The letterhead title is given at a top of each page for easier identification of article copies in an Electronic form in particular. It contains the author's surname and first name initial .article title, journal title and collation (year, volume, and issue, first and last page). The journal and article titles can be given in a shortened form.

Author's Name

Full name(s) of author(s) should be used. It is advisable to give the middle initial. Names are given in their original form.

Contact Details

The postal address or the e-mail address of the author (usually of the first one if there are more Authors) is given in the footnote at the bottom of the first page.

Type of Articles

Classification of articles is a duty of the editorial staff and is of special importance. Referees and the members of the editorial staff, or section editors, can propose a category, but the editor-in-chief has the sole responsibility for their classification. Journal articles are classified as follows:

Scientific articles:

1. Original scientific paper (giving the previously unpublished results of the author's own research based on management methods).
2. Survey paper (giving an original, detailed and critical view of a research problem or an area to which the author has made a contribution visible through his self-citation);
3. Short or preliminary communication (original management paper of full format but of a smaller extent or of a preliminary character);
4. Scientific critique or forum (discussion on a particular scientific topic, based exclusively on management argumentation) and commentaries. Exceptionally, in particular areas, a scientific paper in the Journal can be in a form of a monograph or a critical edition of scientific data (historical, archival, lexicographic, bibliographic, data survey, etc.) which were unknown or hardly accessible for scientific research.

Professional articles:

1. Professional paper (contribution offering experience useful for improvement of professional practice but not necessarily based on scientific methods);
2. Informative contribution (editorial, commentary, etc.);
3. Review (of a book, software, case study, scientific event, etc.)

Language

The article should be in English. The grammar and style of the article should be of good quality. The systematized text should be without abbreviations (except standard ones). All measurements must be in SI units. The sequence of formulae is denoted in Arabic numerals in parentheses on the right-hand side.

Abstract and Summary

An abstract is a concise informative presentation of the article content for fast and accurate Evaluation of its relevance. It is both in the Editorial Office's and the author's best interest for an abstract to contain terms often used for indexing and article search. The abstract describes the purpose of the study and the methods, outlines the findings and state the conclusions. A 100- to 250-Word abstract should be placed between the title and the keywords with the body text to follow. Besides an abstract are advised to have a summary in English, at the end of the article, after the Reference list. The summary should be structured and long up to 1/10 of the article length (it is more extensive than the abstract).

Keywords

Keywords are terms or phrases showing adequately the article content for indexing and search purposes. They should be allocated heaving in mind widely accepted international sources (index, dictionary or thesaurus), such as the Web of Science keyword list for science in general. The higher their usage frequency is the better. Up to 10 keywords immediately follow the abstract and the summary, in respective languages.

Acknowledgements

The name and the number of the project or programmed within which the article was realized is given in a separate note at the bottom of the first page together with the name of the institution which financially supported the project or programmed.

Tables and Illustrations

All the captions should be in the original language as well as in English, together with the texts in illustrations if possible. Tables are typed in the same style as the text and are denoted by numerals at the top. Photographs and drawings, placed appropriately in the text, should be clear, precise and suitable for reproduction. Drawings should be created in Word or Corel.

Citation in the Text

Citation in the text must be uniform. When citing references in the text, use the reference number set in square brackets from the Reference list at the end of the article.

Footnotes

Footnotes are given at the bottom of the page with the text they refer to. They can contain less relevant details, additional explanations or used sources (e.g. scientific material, manuals). They cannot replace the cited literature.

The article should be accompanied with a cover letter with the information about the author(s): surname, middle initial, first name, and citizen personal number, rank, title, e-mail address, and affiliation address, home address including municipality, phone number in the office and at home (or a mobile phone number). The cover letter should state the type of the article and tell which illustrations are original and which are not.

Notes: